Computational Design of Creep-Resistant Alloys and Experimental Validation in Ferritic Superalloys

Investigators: Peter K. Liaw[1], Mark D. Asta[2], Gautam Ghosh[3], David C. Dunand[3], Morris E. Fine[3], Yanfei Gao[1], and Chain T. Liu[4]

Ph.D. Students: Hong Ding[2], Dr. Sharon Huang[1], Michael Rawlings[3], Gian Song[1], Zhiqian Sun[1], and Dr. Kevin Teng[1]

Research Associates: Gongyao Wang[1] and Christian Liebscher[2]

1. Department of Materials Science and Engineering, The University of Tennessee (UT), Knoxville, TN 37996, USA
2. Department of Materials Science and Engineering, University of California (UC), Berkeley, CA 94720, USA
3. Department of Materials Science and Engineering, Northwestern University (NU), Evanston, IL 60208-3108, USA
4. Department of Materials Engineering, Auburn University, Auburn, AL 36849, USA

Acknowledgements

We are very grateful to:

(1) Richard Dunst,

(2) Veto Cedro,

(3) Nicholas Anderson,

(4) Patricia Rawls, and

(5) Robert Romanosky for their kind support.

(6) National Energy Technology Laboratory (NETL)

   for sponsoring this project.

Outline

☐ Technical Background of the Project

☐ Statement of Project Objectives

☐ Project Tasks

☐ Research Progress

☐ Conclusions

☐ Publications/Presentations

Technical Background of the Project

Ferritic Alloys as Candidates for Steam Turbines

Why B2 or/and $L2_1$ precipitates strengthened ferritic steels?

Fe Matrix — NiAl-type (B2) — Ni_2TiAl-type ($L2_1$) — **Hierarchical Precipitates**
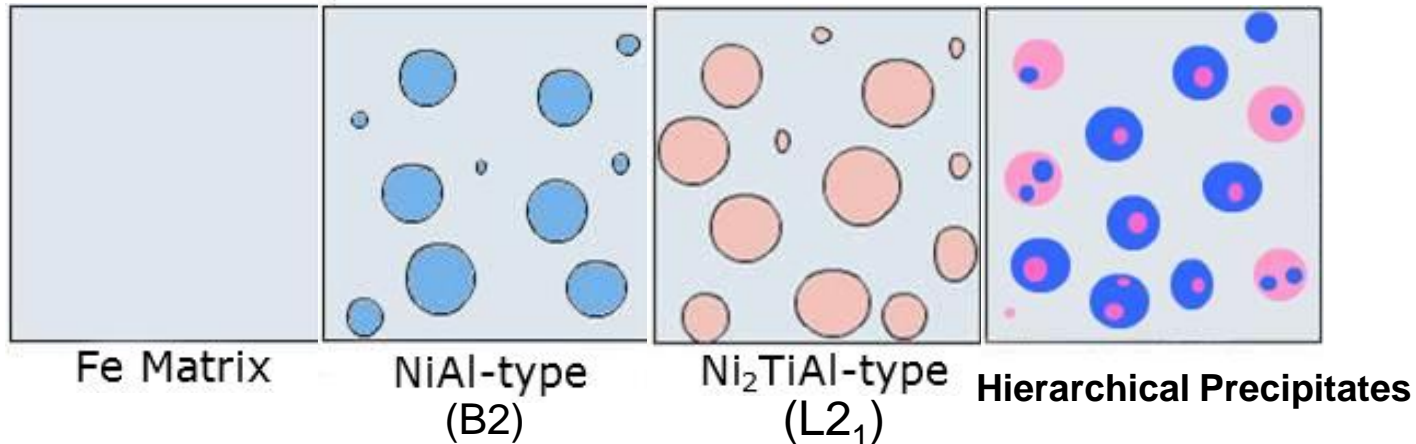
- The elevated-temperature strength of NiAl-type (B2) precipitates is limited by their properties.

- The creep strength (defined as the stress to maintain a steady-state rate of 10^{-7} s^{-1}) of Ni_2TiAl ($L2_1$) between 1,026 to 1,273 K is about three times that of NiAl in its most creep-resistant form.

- The creep strength of NiAl-Ni_2TiAl two-phase alloys are more creep resistant than either of the phases in its monolithic form and at least comparable to the Ni-based superalloy, MAR-M200 (nominal composition wt.%: Cr 9.0; Co 10.0; W 12.5; Nb 1.0; Ti 2.0; Al 5.0; C 0.15; B 0.015; Ni balance).
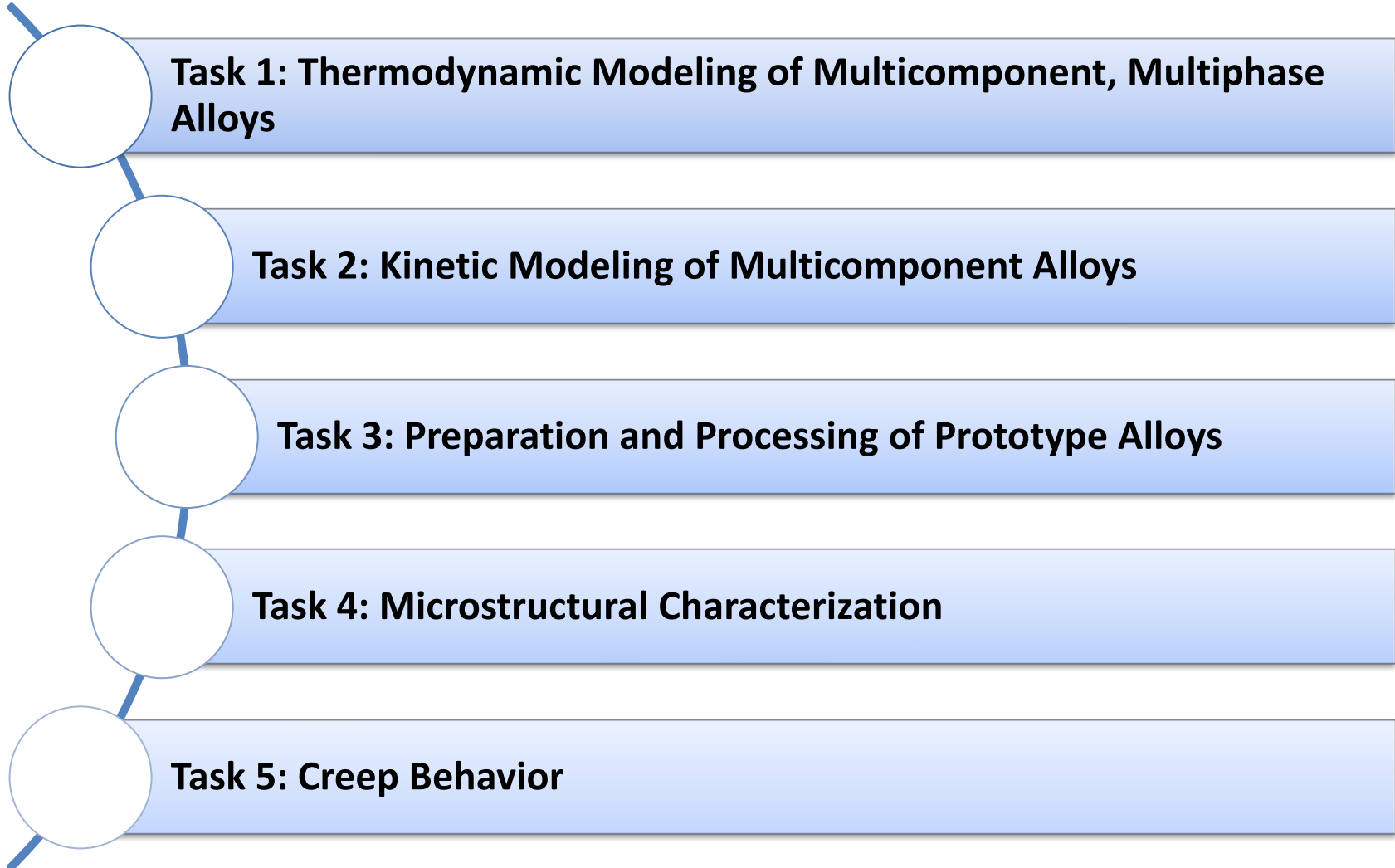
P. R. Strutt, R. S. Polvani, and J. C. Ingram. Metallurgical Transaction A. 7, 23 (1976)
R. S. Polvani, W. S. Tzeng, and P. R. Strutt. Metallurgical Transaction A. 7, 33 (1976)

Project Objectives

- **Objective 1:** to develop and integrate modern computational tools and algorithms required to assist in the optimization of creep properties of high-temperature alloys for fossil-energy applications
  - Integrate tools and methods associated with predictive first-principles calculations, computational thermodynamic and kinetic modeling, and meso-scale dislocation-dynamics simulations.

- **Objective 2:** to achieve a fundamental understanding of the processing-microstructure-property-performance links underlying the creep behavior of novel ferritic superalloys strengthened by *B2 and/or L2$_1$ intermetallics.*
  - Validate some of the computational results by measuring selected microstructural attributes in representative model ferritic superalloys with a hierarchical microstructure.

Project Tasks

Task 1: Thermodynamic Modeling of Multicomponent, Multiphase Alloys

Task 2: Kinetic Modeling of Multicomponent Alloys

Task 3: Preparation and Processing of Prototype Alloys

Task 4: Microstructural Characterization

Task 5: Creep Behavior

Research Progress

1.1 Calculations of Elastic Constants of Fe, *B2*, and *L2*₁ (Heusler) Phases

$$E(V,\{e_i\}) = E(V_0,0) - PV_0 \sum_{i=1}^{3} e_i + \frac{V_0}{2} \sum_{i=1}^{6} \sum_{j=1}^{6} C_{ij} e_i e_j + O[e_i^3]$$

• Fe and *B2* Phases (in GPa)

Phase \\ Elastic Constant	Fe: Cal. (Exp.)	NiAl: Cal. (Exp.)	FeAl: Cal.	CoAl: Cal.
C_{11}	264.37 (243.1*)	207.30 (206.7**)	266.64	292.49
C_{12}	135.10 (138.1*)	135.48 (135.4**)	130.20	123.83
C_{44}	91.21 (121.9*)	116.18 (116.8**)	144.93	135.90

*At 4.2 K: J.A. Rayne and B.S. Chandrasekhar, Phys. Rev., 1960, 120, 1658.
**50 at.% Ni and at 251 K: T. Davenport, L. Zhou and J. Trivisonno, Phys. Rev. B, 1999, 59, 3421.

• Heusler Phases (in GPa)

Phase \\ Elastic Constant	Ni_2TiAl	Fe_2TiAl	Co_2TiAl
C_{11}	211.87	313.75	288.89
C_{12}	143.39	124.07	137.79
C_{44}	87.23	108.77	111.88

- C_{ij}s are obtained by first-principles method: total energy of the system as a function of deformation ($E(V,\{e_i\})$).
- A comparison of calculated C_{ij} of Fe and B2 phases were given previously in a quarterly progress report*.
- There is NO experimental C_{ij} data of Heusler phases, so calculations from first-principles is the only viable option.
- C_{ij} is needed to understand morphology of coherent precipitates and interfacial energy.

* Report_DOE_DE-FE0005868_07292011.pdf

2.1 Model for Self and Impurity Diffusivities

Harmonic Transition State Theory Assuming Vacancy Mechanism

$$D_A^B = D_{0\,A}^{\ B} \exp[-Q_A^B / k_B T]$$

Self Diffusion in α-Fe

$$D_{0\,Fe}^{\ Fe} = a^2 f_{bcc} \exp\left[\frac{\Delta S_v^f}{k_B}\right] x \left[\prod_{i=1}^{3N-3} \nu_i^{vac} \Big/ \prod_{i=1}^{3N-4} \nu_i^{sad}\right] \qquad Q_{Fe}^{Fe} = \Delta H_v^f + \Delta H_v^{mig,Fe}$$

Impurity Diffusion

$$D_{0\,Fe}^{\ I} = a^2 f_{Fe}^I \exp\left[\frac{\Delta S_v^f + \Delta S_v^{bind}}{k_B}\right] x \left[\prod_{i=1}^{3N-3} \nu_i^{vac} \Big/ \prod_{i=1}^{3N-4} \nu_i^{sad}\right] \quad Q_{Fe}^I = \Delta H_v^f + \Delta H_v^{bind} + \Delta H_v^{mig,I}$$

Diffusivity Calculations Require Determinations of:
- Vacancy Formation, Binding and Migration Energies
- Vacancy Formation, Binding and Migration Entropies
- Correlation Factors for Impurity Diffusion

2.2 Diffusivities of 5d Transition Metal Impurities In α-Fe

Solute-vacancy binding enthalpy ΔH_m and the ferromagnetic Q^F in α–Fe all in units of eV, are in the first three rows, respectively. The QP is derived as $Q^P = Q^F / (1+ \alpha)$. The correlation factors, f_2, and diffusion pre-exponential factors, D_0 (mm^2/s) obtained by Le Claire's model, corresponding to 1,000K, are listed in the last two rows.

Energy/Factor \ Element	Ta	W	Re	Os	Ir	Pt	Au
ΔH_b (Binding energy)	-0.33	-0.17	-0.13	-0.13	-0.16	-0.28	-0.32
ΔH_m (Migration energy)	0.43	0.71	0.86	0.90	0.88	0.85	0.76
Q^F (Ferromagnetic Activation Energy)	2.30	2.74	2.93	2.97	2.92	2.77	2.64
α (Magnetic Effect factor)	0.06	0.09	0.08	0.12	0.18	0.24	0.25
Q^P (Paramagnetic Activation Energy)	2.17	2.52	2.71	2.65	2.48	2.23	2.11
f_2 (Correlation Factor : 1,000 K)	0.03	0.73	0.93	0.97	0.96	0.90	0.57
D_0 (Diffusion Constant : 1,000 K)	4.04	138	298	310	118	67	21

- Relative values of diffusion coefficient accurate than the absolute values
- Three groups for diffusivities (*D* in a paramagnetic state)
  - *Faster:*   *Pt* and *Au*
  - *Close:*   *W, Ir,* and *Ta*
  - *Slower:*   *Re* and *Os*
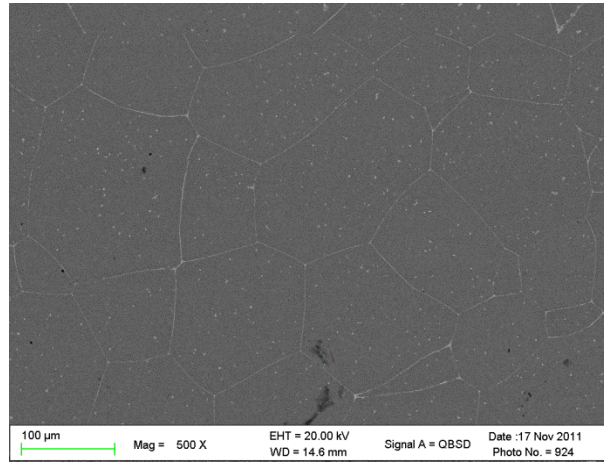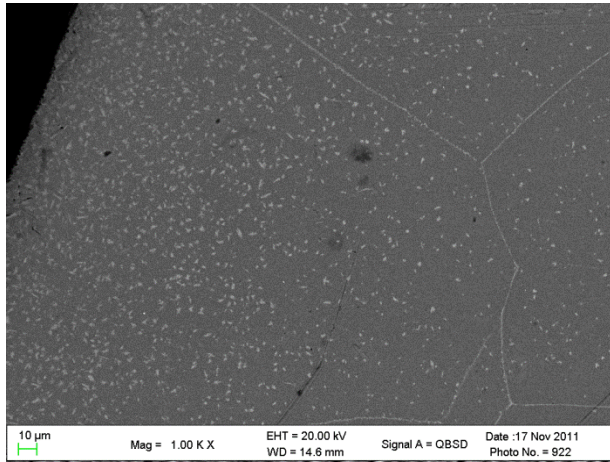
Fe-2Ti-6.5Al-10Cr-10Ni-3.4Mo-0.25Zr- 0.005B, wt.%
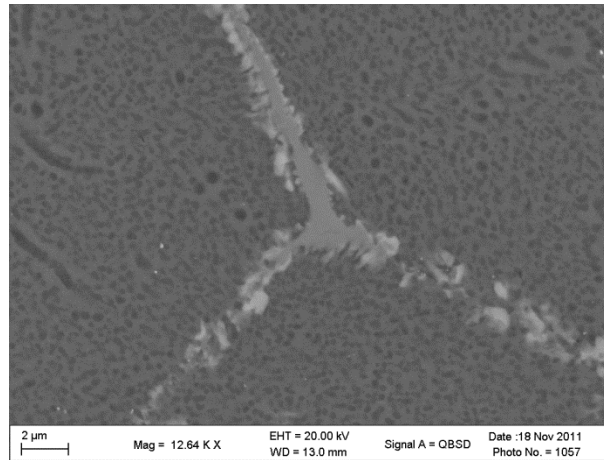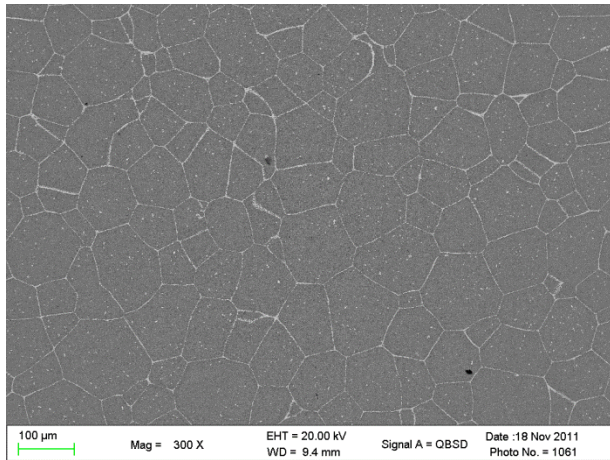
Fe-6Ti-6.5Al-10Cr-10Ni-3.4Mo-0.25Zr- 0.005B, wt.%

Heat treatments (30 min. at 1,523 K + air cooling + 100 hours at 973 K + air cooling).

- **Segregation (white) areas are found in grains and along grain boundaries**
- **EDS results reveal that segregation areas are rich in Mo and Zr.**

4.1 Microstructural Characterization-On the Formation of Hierarchical $L2_1$-Precipitates

TEM diffraction pattern showing reflections of both $B2$ and $L2_1$ type structures

Alloy composition: Fe-8.08Al-12.2Cr-1.9Mo-18.2Ni-4Ti (wt. %)
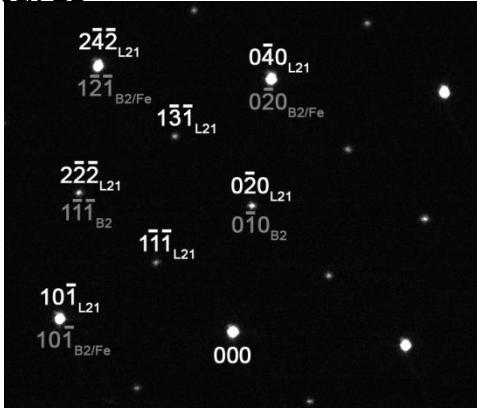
TEM dark field image using (111)-type $L2_1$ reflection

TEM dark field image using (222)-type $B2/L2_1$ reflection

TEM dark field using (111)- type $L2_1$ spots
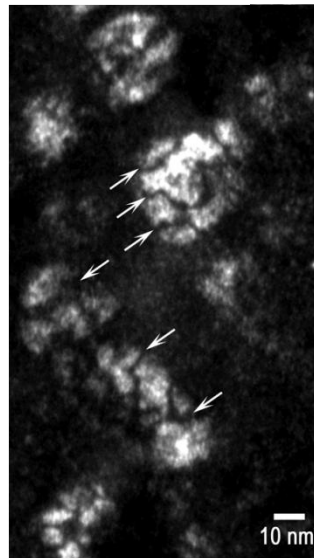
Proof of the formation of (100)-type APBs within $L2_1$-precipitates

TEM dark field using (020)-type $B2/L2_1$ spots

14

Heat treated state after annealing at 700˚C for 10 h:

TEM dark field using (020)- type $B2/L2_1$ spots
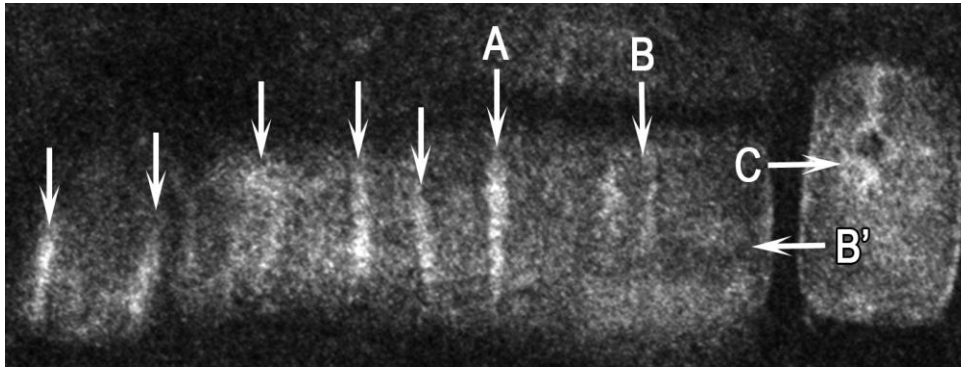
TEM dark field using (111)- type $L2_1$ reflection
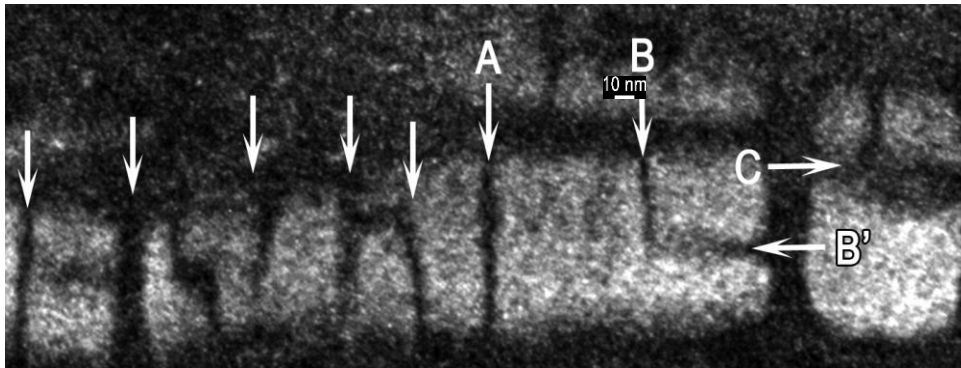
TEM dark field image using (222)- type $B2/L2_1$ reflection
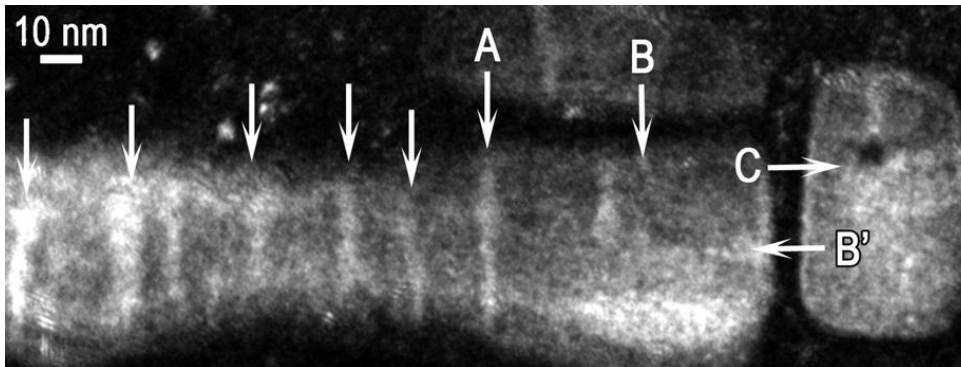
Zones with brighter contrast than $L2_1$-precipitate and a width of 3-5 nm visible imaging with $B2/L2_1$-spots

Clear indication of B2-formation within $L2_1$-precipitates

Alloy composition: Fe-8.08Al-12.2Cr-1.9Mo-18.2Ni-4Ti (wt. %)

15

Local Electrode Atom Probe (LEAP)/Atom Probe Tomography (APT) Map

92 nm · 92 nm · 92 nm

Sc atoms

394 nm

394 nm

Al-2.9 Li-0.11 Sc
325 °C 9.5 min
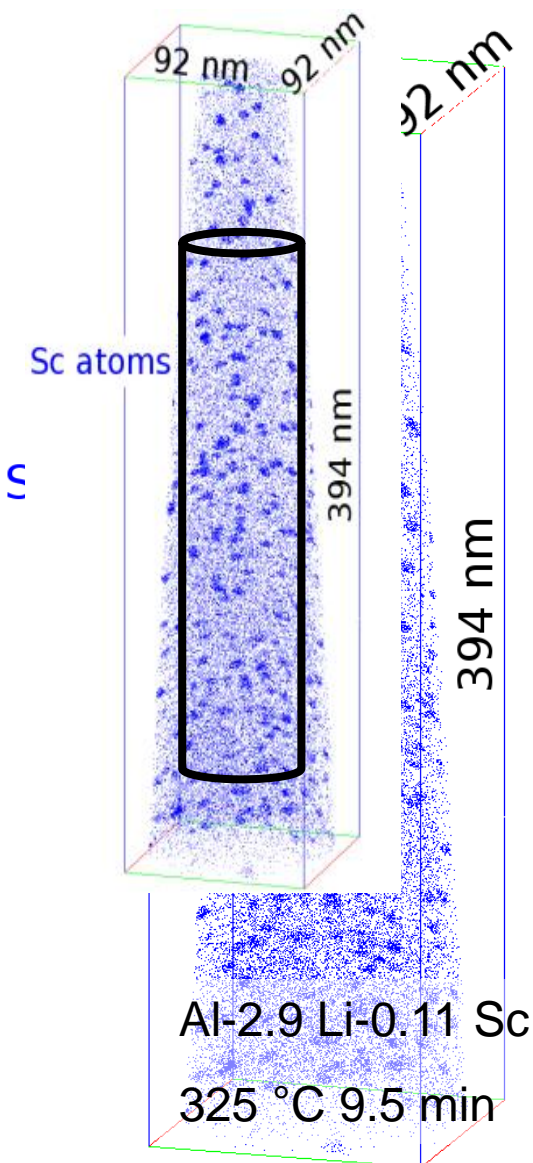
1. Isolate precipitates- cluster search algorithm:

   Each precipitate i : (x_i y_i z_i r_i)

2. Find the largest inscribed cylinder

3. Apply random symmetry operations:

   rotations, mirrors, translations

4. Assemble resulting cylinders

5. Cut through common plane to create glide plane

τ

Slide courtesy: Matt Krug, NU

16
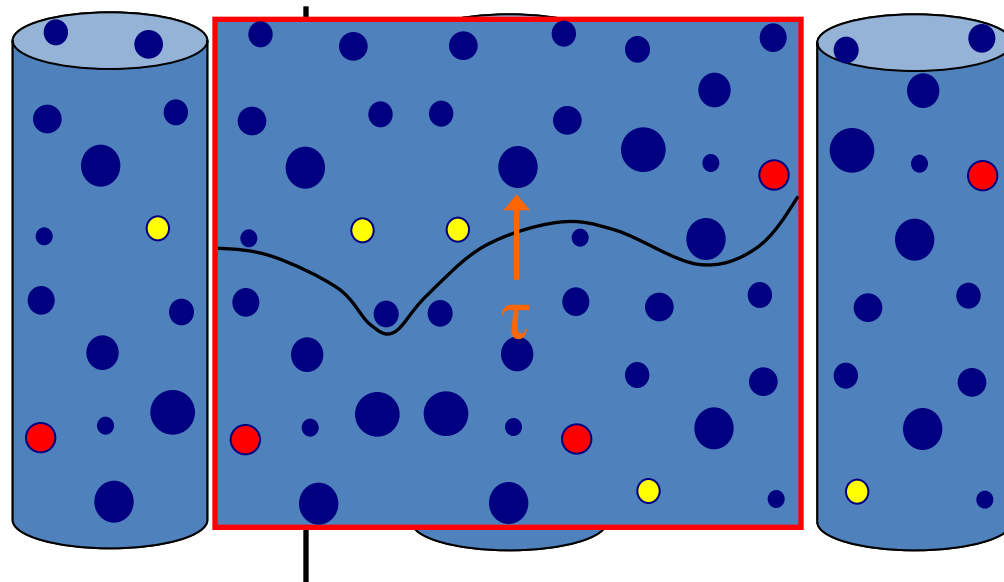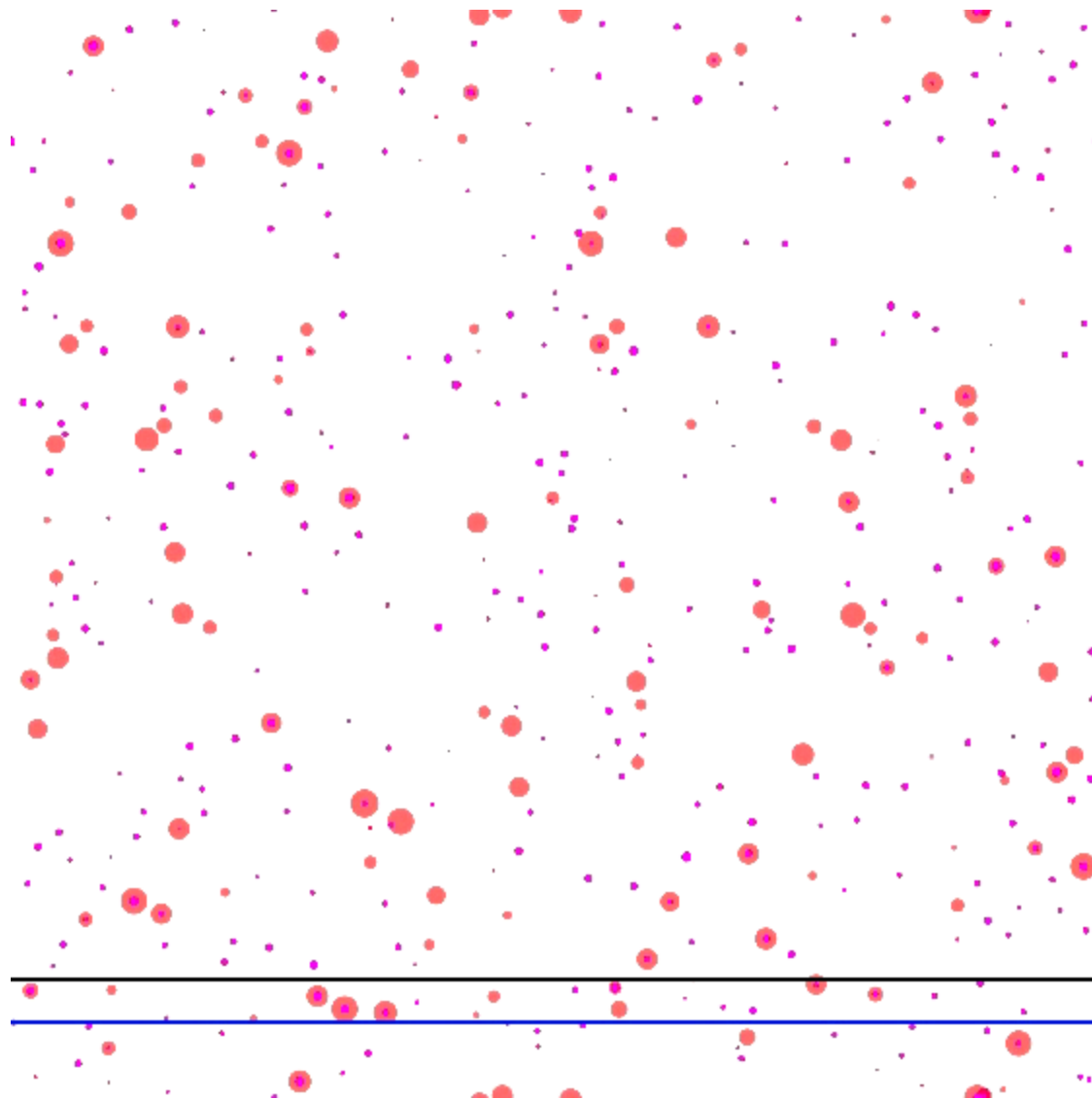
8h 325C
20h 170C

fc = 0.820%
fs = 2.062%
rc = 2.3 nm
rs = 7.3 nm
  b ↑

s = 16.000

a = 0.090

N = 2

00:00.00

M. Krug 2011
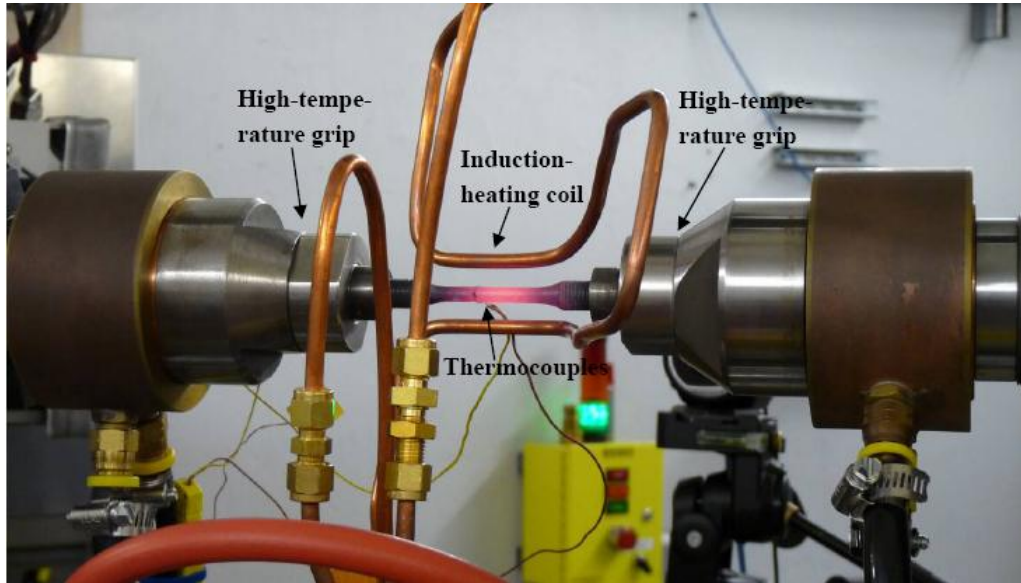Materials Science
Northwestern U

Video courtesy: Matt Krug, NU

Spallation Neutron Source (SNS), Oak Ridge National Laboratory (ORNL)

Conceptual design of VULCAN diffractometer

The multifunctional load-frame developed for VULCAN diffractometer
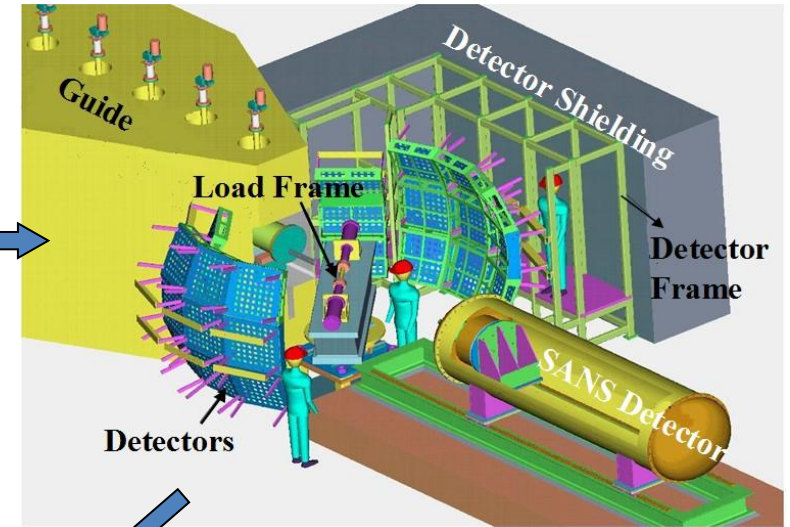
Motivation

- Reveal intergranular and interphase load partition
- Validate crystal-plasticity finite-element simulation

Materials

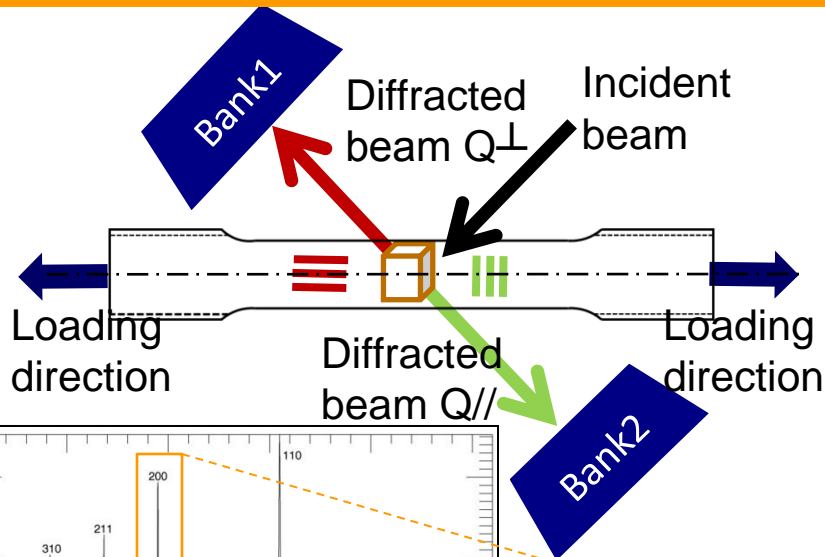- Fe-6.5Al-10Cr-10Ni-3.4Mo-0.25Zr-0.005B (wt.%)
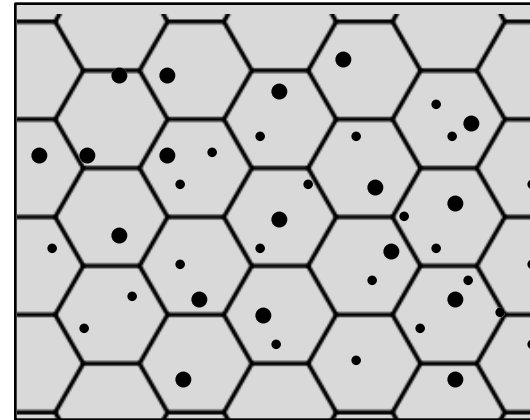- Aged condition

Experiments at VULCAN, SNS, ORNL

- Quasi-static tension under load control
- Induction heating in air
- Macroscopic strain measured by room-temperature extensometer, and by cross-head displacement at elevated temperatures
- 40 minutes batch for each stress level
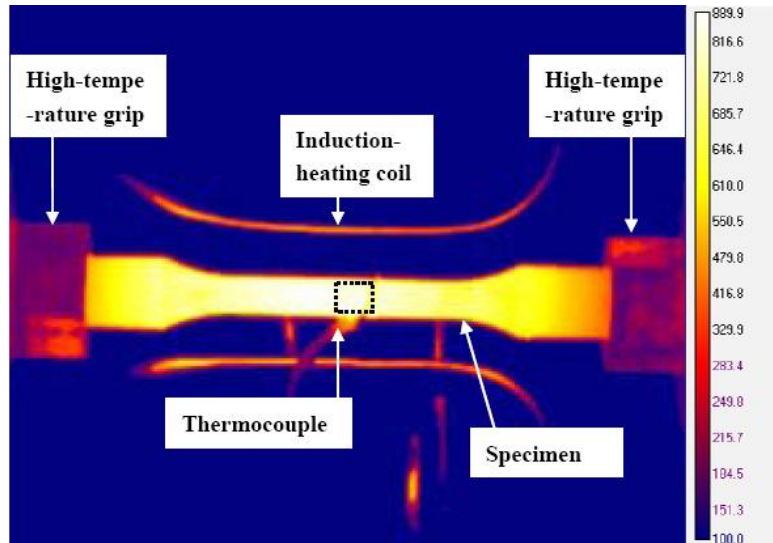
Infrared camera measures temperature variation ~10 K inside neutron beam

6.1 In-situ Neutron Diffraction Probes Structural Changes

Bank1

Diffracted beam Q⊥

Incident beam

Loading direction

Diffracted beam Q//

Loading direction

Bank2

1. Volume-averaged phase strain

$$\varepsilon_{avg\_phase} = \frac{a - a_0}{a_0}$$

Rietveld whole-pattern fitting

500C Tension 600 MPa (200) Peak Separation
□ Measured data
— Fitted
— matrix β
— precipitate β'
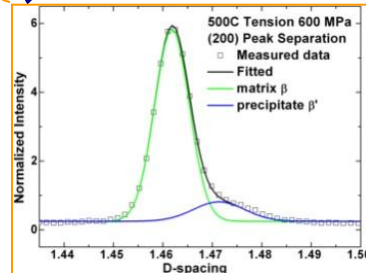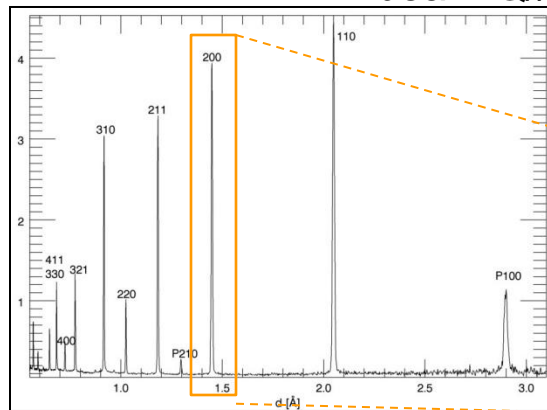
2. hkl-plane specific strain–intergranular
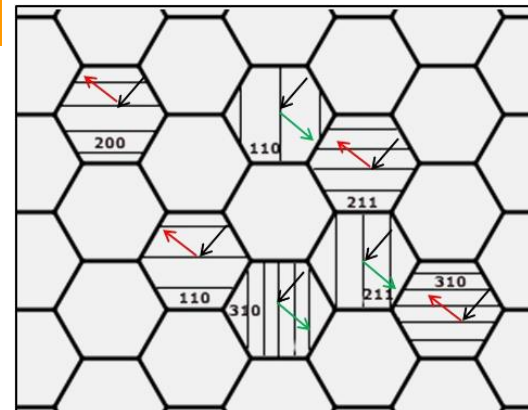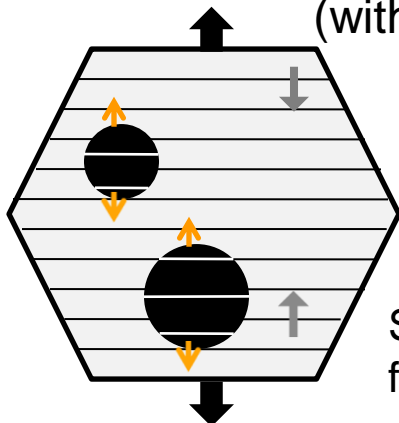
$$\varepsilon_{hkl} = \frac{d_{hkl} - d_{hkl}^0}{d_{hkl}^0}$$

single peak fitting of overlapping composite peak

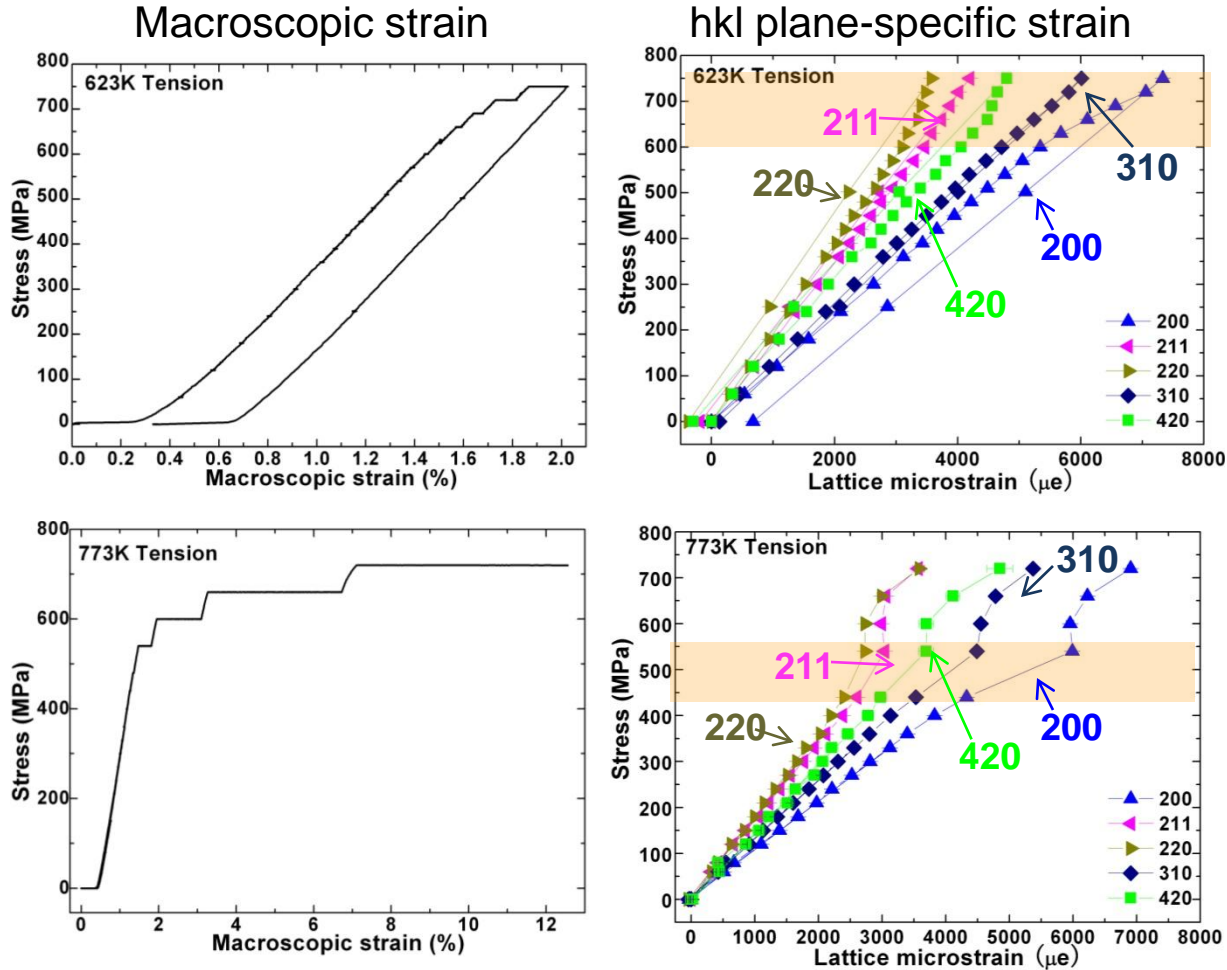## 3. Local phase strain-intragranular

(within hkl grain family)

$$\varepsilon_{local\_\beta} = \frac{d_{hkl}^{\beta} - d_{hkl}^{\beta,0}}{d_{hkl}^{\beta,0}}$$
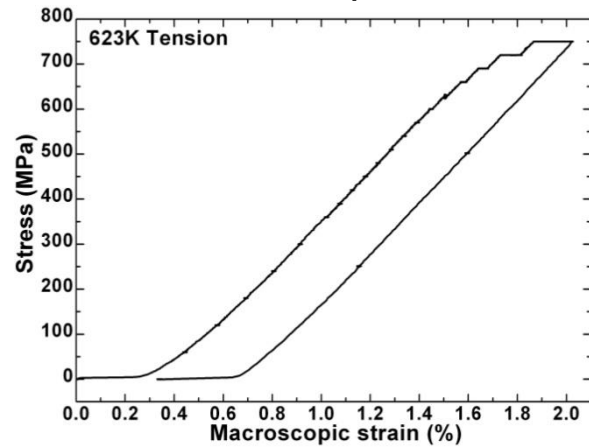
Separation of overlapping fundamental reflections

6.2 Tension at 623 and 773 K – Intergranular and Interphase Load Transfer

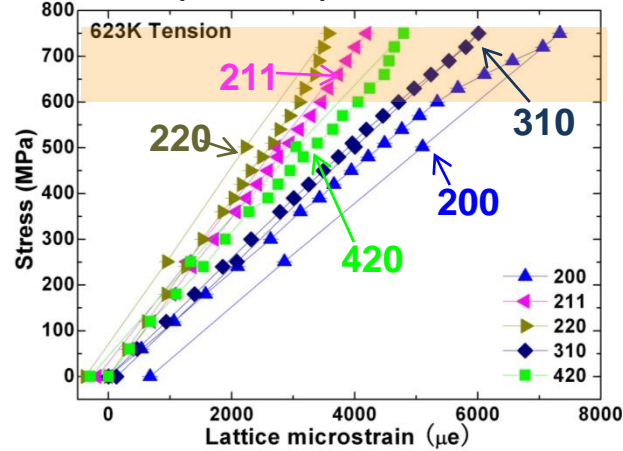Macroscopic strain

hkl plane-specific strain

- The onset of plastic deformation is marked by deviation from linear response
- Plastic anisotropy: plastic deformation occurs on certain preferential slip systems, and the sequence of grain yielding relies on Schmid factor
- 110 and 420 oriented grains yield first with load transfer to 200 grains.

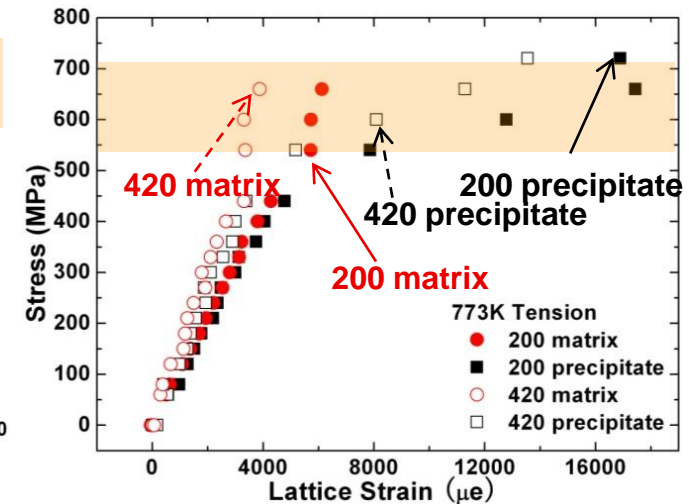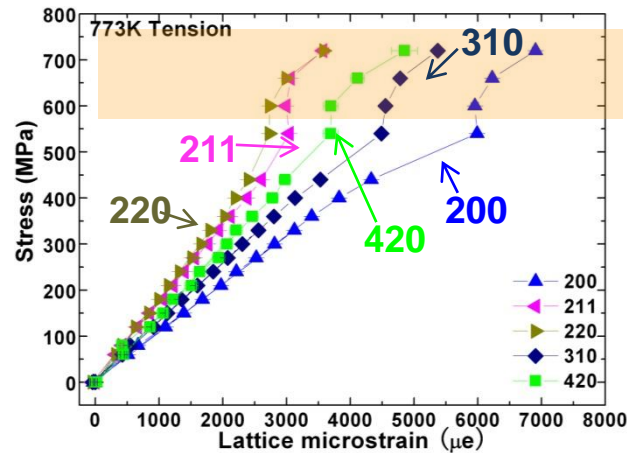# 6.2 Tension at 623 and 773 K – Intergranular and Interphase Load Transfer

Macroscopic strain | hkl plane-specific strain | Local phase lattice strain

- Interphase load transfer is superimposed on the intergranular load transfer.

- There is dramatic load transfer from matrix to precipitate phase at 773K, after yielding of most similarly oriented hkl grain families.
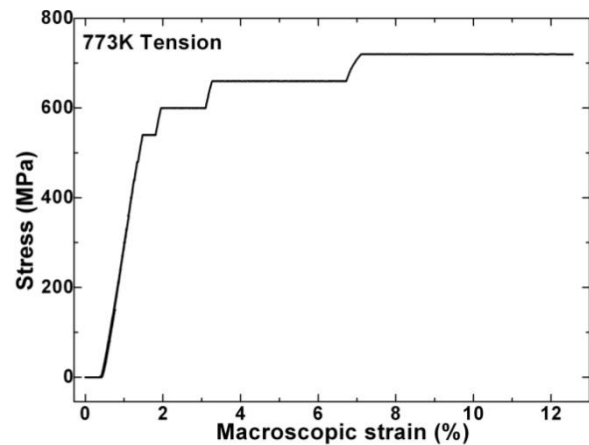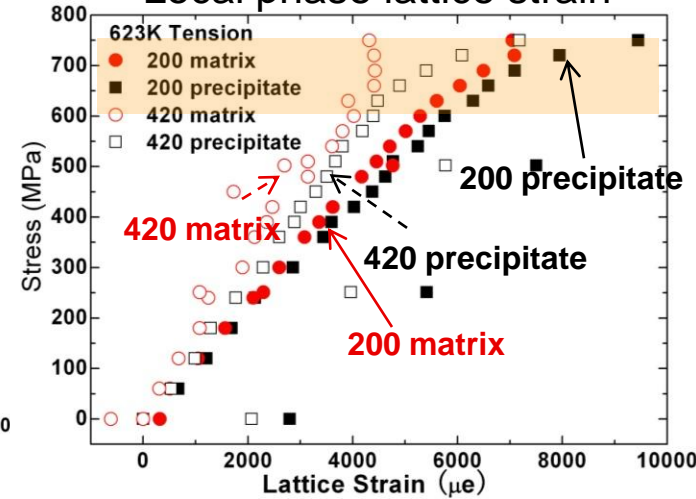
6.3 In-situ Tension at 873 and 973 K

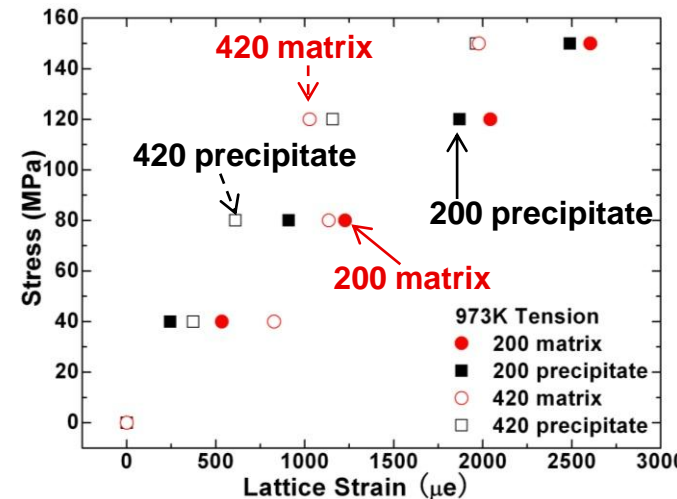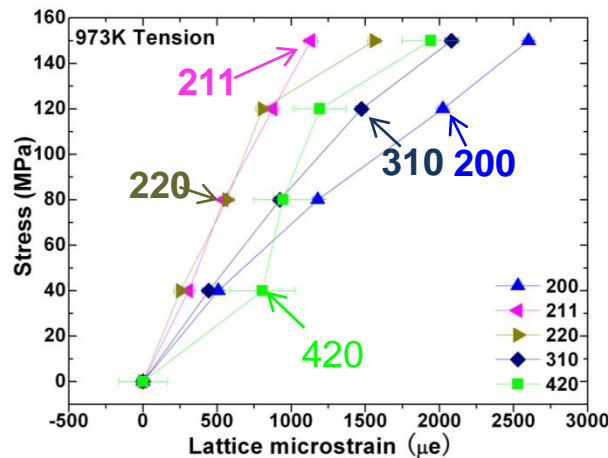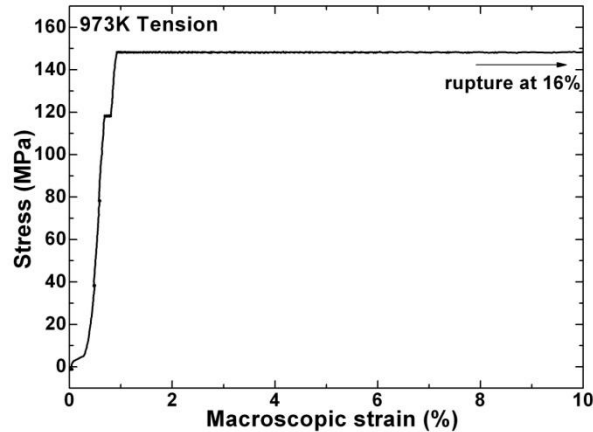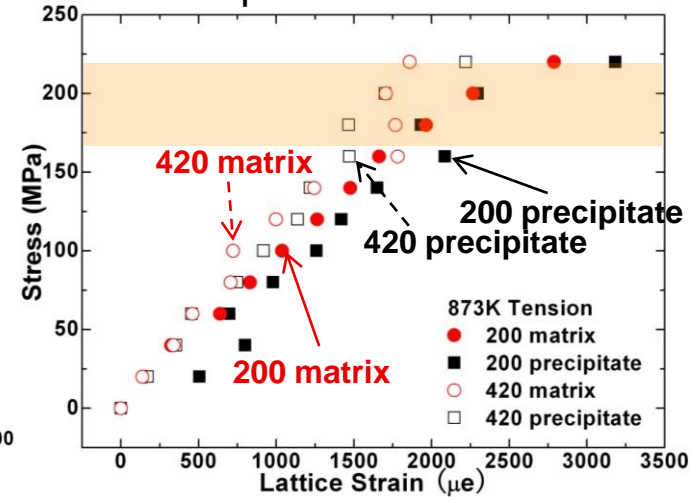| Macroscopic strain	hkl plane-specific strain	Local phase lattice strain
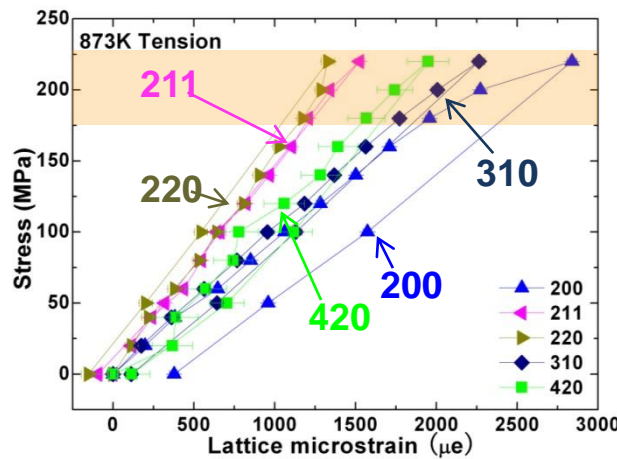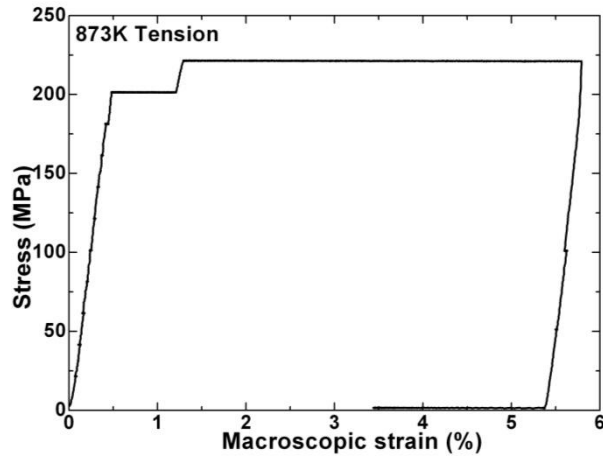
- At 973 K, macroscopic strain increases substantially at high stress levels due to creep. There is no obvious evidence of intergranular and interphase load transfer.

6.5 Crystal-Plasticity Finite-Element Model (CPFEM)

□ **Multiplicative decomposition**

$$F = F^e F^p$$

$$F_{ij} = \partial x_i / \partial X_j = F_{ik}^e F_{kj}^p$$

elastic $\quad T_{ij} = C_{ijkl} E_{kl}^e$

plastic $\quad \dot{F}_{ik}^p F_{kj}^{p-1} = \sum_{\alpha=1}^{N_{SLIP}} \dot{\gamma}^{(\alpha)} s_i^{(\alpha)} m_j^{(\alpha)}$

□ **Flow rule**

$$\dot{\gamma}^\alpha = \dot{\gamma}^0 \left(\frac{\tau^\alpha}{g^\alpha} \right)^N$$

$$\tau^\alpha = m_i^\alpha F_{ij}^{e-1} J \sigma_{jk} F_{kl}^e s_l^\alpha$$

□ **Hardening law**

$$\dot{g}^\alpha = \sum_\beta h_{\alpha\beta} |\dot{\gamma}^\beta|$$

$$h_{\alpha\beta} = h_{\alpha\alpha} \left[q + (1-q) \delta_{\alpha\beta} \right]$$

$\dot{\gamma}^0$: characteristic strain rate

τ^α : resolved shear stress of α slip system

g^α : flow strength of α slip system

N : stress exponent

$h_{\alpha\beta}$: hardening moduli

$h_{\alpha\alpha}$: self - hardening moduli

q : latent hardening coefficient

h_0 : initial hardening modulus

τ_0 : initial slip strength

τ_s : saturation slip strength
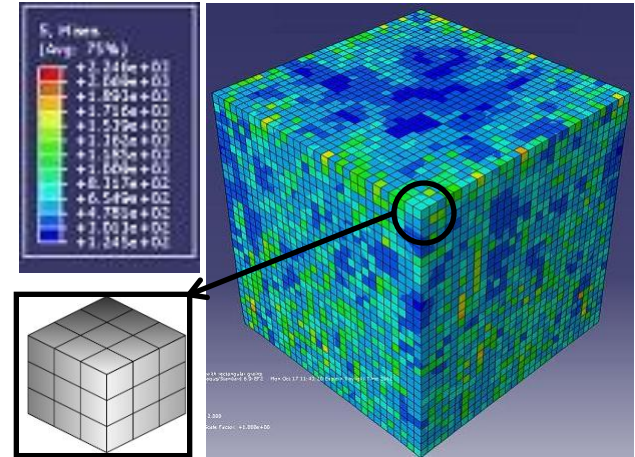
1,000 cubic grains, random texture
3 x 3 x 3 grid, Vol.% = 18.5%

<100>pole figure for 1000 grains
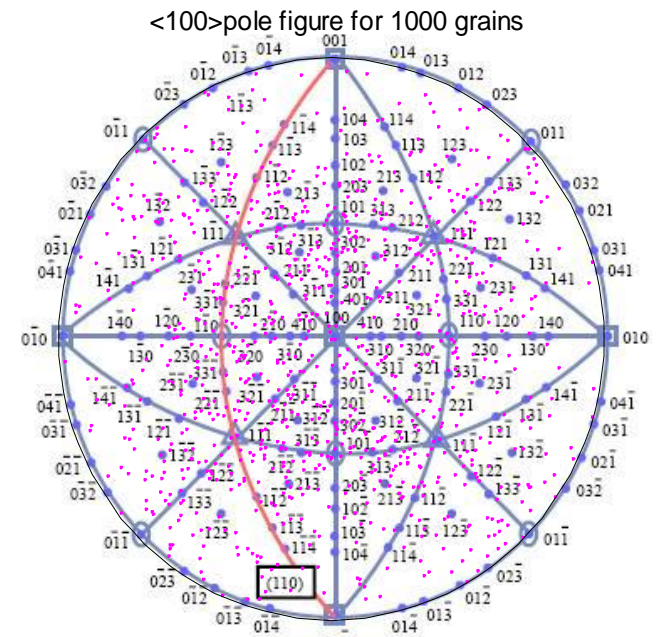
[1] Peirce D, Asaro RJ, Needleman A. Acta Metallurgica 1982;30:1087.
[2] Bower AF, Wininger E. J. Mech. Phys. Solids 2004;52:1289.
[3] Zheng LL, Gao YF, Lee SY, Barabash RI, Lee JH, Liaw PK. J. Mech. Phys. Solids (2011), doi:10.1016/j.jmps.2011.08.001 .

The model predicts well in
- ☐ elastic regime
- ☐ elastic-plastic transition
- ☐ interphase load transfer
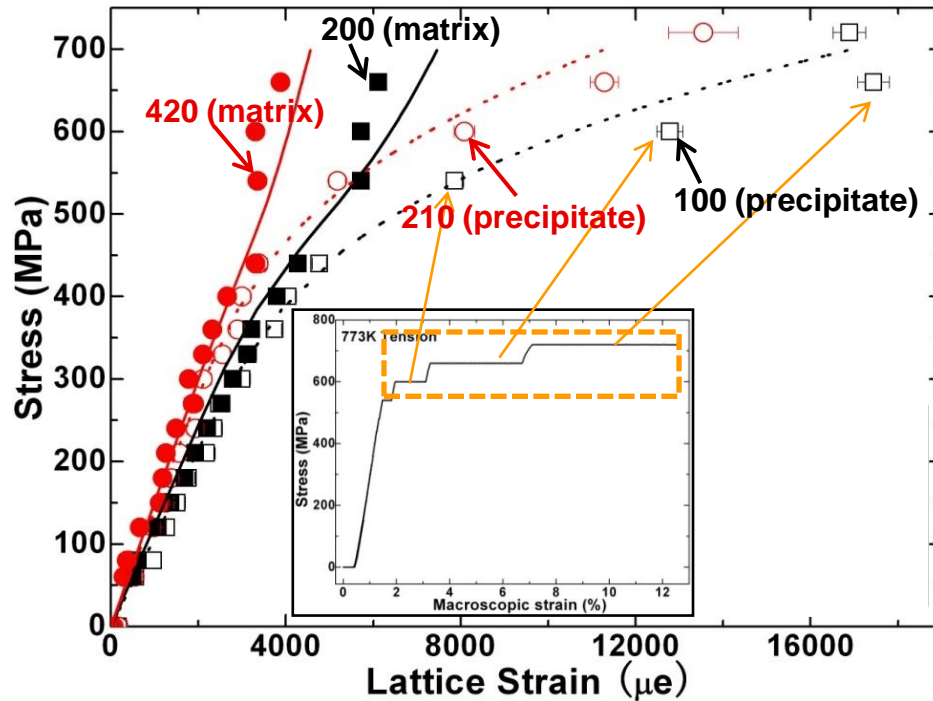
Modified model with creep effects during stress hold
- ☐ Improved prediction of precipitates lattice strains at high stress
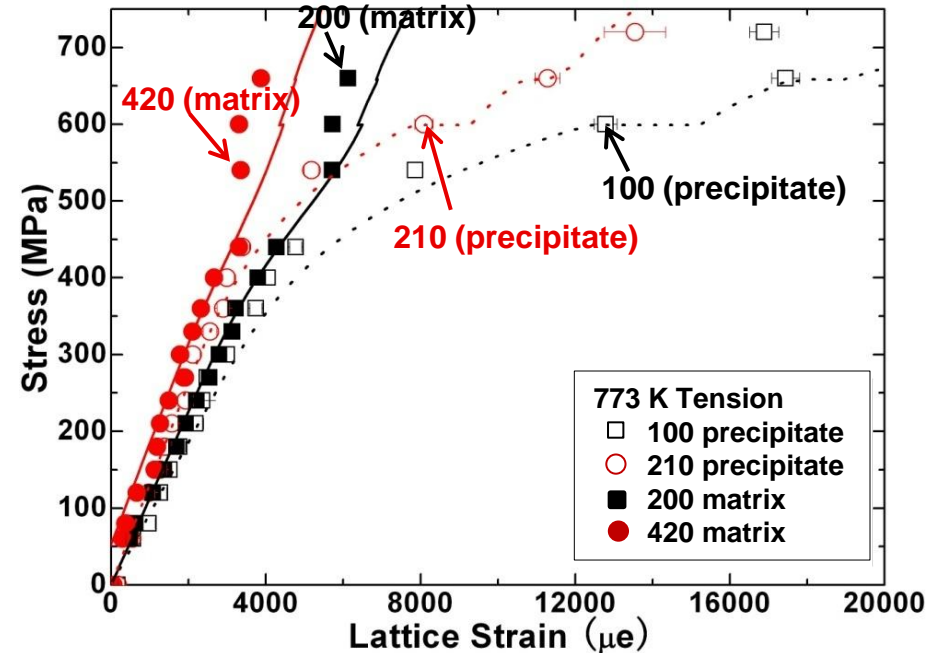
	C_{11} (GPa)	C_{12} (GPa)	C_{44} (GPa)	T_0 (MPa)	T_s (MPa)	N	H_0	q
Matrix	198	164	98	150	157	10	100	1.0
Precipitate	190	165	106	500	800	10	100	1.0

- ☐ **CPFEM shows qualitative agreement with neutron-diffraction results.**

25

7. Future work

- Integration of Computational Thermodynamics and Kinetics including NiAl-type B2 precipitates will be extended to include the Heusler phase as a precipitate and incorporated in the Thermo-Calc database.

- Free-energy contributions due to thermal expansion, phonon, electronic excitations, and magnetic disordering will be considered in order to compute the temperature dependence of elastic constants

- The microstructure characterization will be performed using high-resolution analytical-electron microscopy, local electrode atom probe, transmission electron microscopy and neutron/synchrotron facilities. We will investigate the relationship between the microstructure and creep strength of the material.

- (1) The creep and tensile experiments, (2) in-situ creep neutron-diffraction measurements, and (3) theoretical creep simulations based on dislocation dynamics will be integrated to predict the optimal creep strength with optimized microstructural parameters (e.g., precipitate size, volume fraction, spatial distribution, APB energies, and lattice mismatch)

Conclusions

1. **Calculations of Elastic Constants**
   - Single-crystal elastic constants (Cij) of Fe and relevant B2 phases are calculated from first-principles. They show a good agreement with experimental data, where available.
   - There is no experimental Cij data of Heusler phases. Thus, calculations from first-principles are the only viable option.

2. **Kinetic Modeling of Multicomponent Alloys**
   - First-principles methods have been conducted to predict diffusivities in dilute body-centered cubic (bcc)-Fe solutions.

3. **Microstructural Characterization (High-Resolution TEM)**
   - $L2_1$-precipitates and a fine network of isotropic 100-type APBs within $L2_1$-precipitates are present in the as-quenched alloy.
   - B2-NiAl and residual 100-type APBs form within $L2_1$-precipitates in the heat-treated alloy.

Conclusions (Cont'd)

4. Preparation and Processing of Prototype Alloys

- Segregation in new-designed alloys with Ti contents may have significant impacts on mechanical properties of ferritic alloys.

5. Neutron-Diffraction Measurements

- Below 773 K, intergranular and interphase load transfer are observed in the plastic regime, following the dislocation slip mechanism.
- Above 873 K, intergranular and interphase load transfer are not obvious in the plastic regime; the material undergoes power-law creep possibly due to grain-boundary sliding or diffusional flow.
- Crystal-plasticity finite-element simulations show reasonably good agreement with neutron-diffraction measurements.

Papers and Presentations

- ## Papers
  1) Z.K. Teng, M.K. Miller, G. Ghosh, C.T. Liu, S. Huang, K.F. Russel, M.E. Fine, and P.K. Liaw, Scripta Materialia, 2010;63:61.
  2) S. Huang, D.L. Worthington, M. Asta, V. Ozolins, G. Ghosh, and P.K. Liaw, Acta Materialia, 2010;58:1982.
  3) S. Huang, B. Clausen, D. Brown, Z.K. Teng, Y.F. Gao, and P.K. Liaw, Metallurgical and Materials Transactions A, 2012;43;1497.
  4) Z.K. Teng, F. Zhang, M.K. Miller, C.T. Liu, S. Huang, Y.T. Chou, R.H. Tien, Y.A. Chang, and P.K. Liaw, Materials Letters, 2012;71;36-40.
  5) Z.K. Teng, C.T. Liu, M.K. Miller, G. Ghosh, E.A. Kenik, S. Huang, and P.K. Liaw, Materials Science and Engineering A, 2012;541;22.
  6) H. Ding, S. Huang, G. Ghosh, P.K. Liaw, and M. Asta, submitted to Scripta Mater.
  7) S. Huang, G. Ghosh, X. Li, J. Ilavsky, Z.K. Teng, and P.K. Liaw, submitted to Metallurgical and Materials Transactions A.
  8) S. Huang, Y.F. Gao, K. An, W. Wu, L. Zheng, M. Rawlings, D.C. Dunand, and P.K. Liaw, in preparation for Acta Materialia.
  9) C. H. Liebscher, V. Radmilovic, U. Dahmen, M. Asta and G. Ghosh, in preparation

- ## Presentations
  1) S. Huang, Y.F. Gao, K. An, W. Wu, L. Zheng, M. Rawlings, D. Dunand, P.K. Liaw, TMS 141th Annual Meeting, Orlando, FL, Mar., 2012, 03/11 - 03/15.
  2) C.H. Liebscher, V. Radmilovic, U. Dahmen, M. Asta, G. Gosh, Microscopy & Microanalysis 2012 Meeting, at the Phoenix Convention Center in downtown Phoenix, AZ., 2012, 07/29 - 08/02.
  3) C.H. Liebscher, V. Radmilovic, U. Dahmen, M. Asta, G. Gosh, Materials Science and Technology 2012 Meeting, Pittsburgh, Pennsylvania, 2012, 10/07 - 10/11.
  4) H. Ding, S. Huang, G. Ghosh, P.K. Liaw, M. Asta, Materials Science and Technology 2012 Meeting, Pittsburgh, Pennsylvania, 2012, 10/07 - 10/11.

Structure of B2 (NiAl) and L2$_1$ (Ni$_2$TiAl) phases


Ni$_2$TiAl

NiAl

31
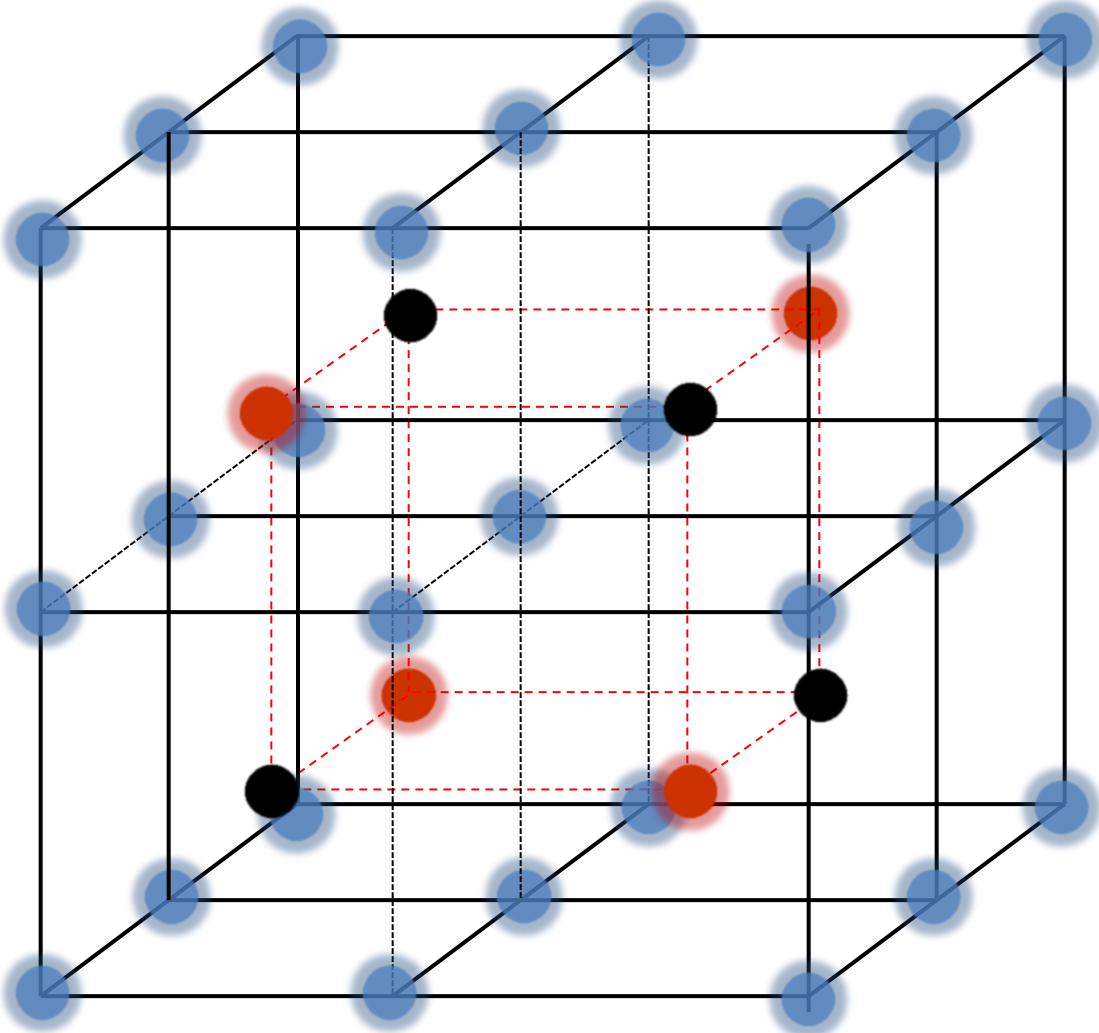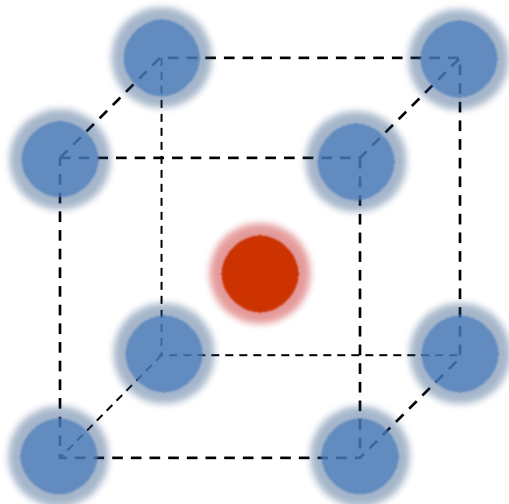
Proposed Research and Progress

Ferritic Alloys as Candidates for Steam Turbine (1)

Why ferritic steels? Why not Ni-based alloys?

- 80% of all electricity generation in the world is by use of steam turbines. Low cost materials are required.

- The materials with good thermal conductivity and low thermal expansion are preferable for thick section components of the steam turbine.

	Thermal Expansion Coefficient [2]	Thermal Conductivity[3]	Cost ($/t) [4]
Ferritic steel	1.0×10^{-5} K^{-1}	50 W/(m·K)	< $900
Ni-based superalloy	1.8×10^{-5} K^{-1}	21 W/(m·K)	> $40K
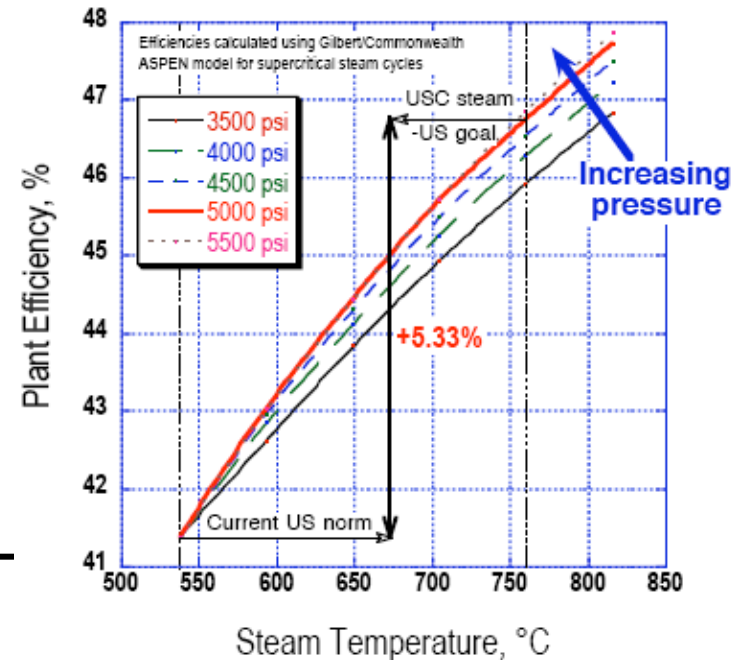
P. Maziasz, I. Wright, J. Shingledecker, T. Gibbons, R. Romanosky, *Proceedings from the fourth international conference on advances for materials technology for fossil power plants* 2005.

[1] http://en.wikipedia.org/wiki/Steam_turbine
[2] http://www.handyharmancanada.com/TheBrazingBook/comparis.htm
[3] http://en.wikipedia.org/wiki/List_of_thermal_conductivities
[4] http://www.ttiinc.com/page/ME_Materials

Ferritic Alloys as Candidates for Steam Turbine (2)

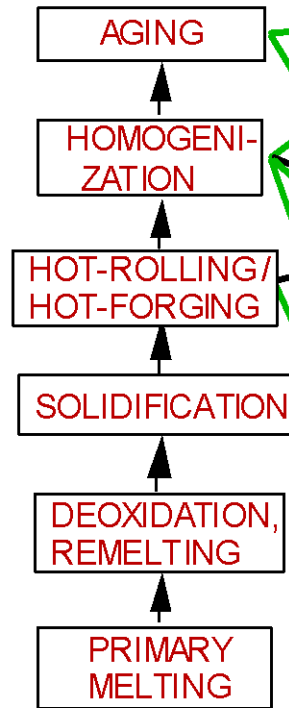## Why B2 or/and L2$_1$ precipitates strengthened ferritic steels?

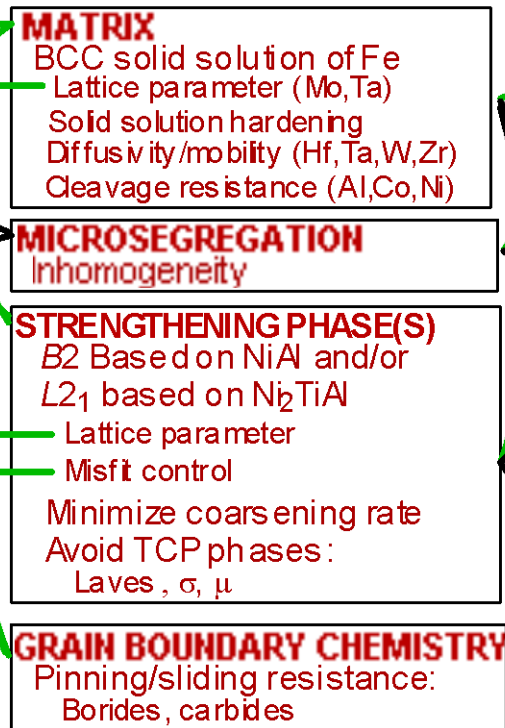| Phase	Structure	Lattice Parameter (nm)
α-Fe	Body-Centered-Cubic (BCC)	0.28665
NiAl	B2 (ordered BCC)	0.28864
FeAl	B2 (ordered BCC)	0.289
Ni$_2$TiAl	L2$_1$	0.5865
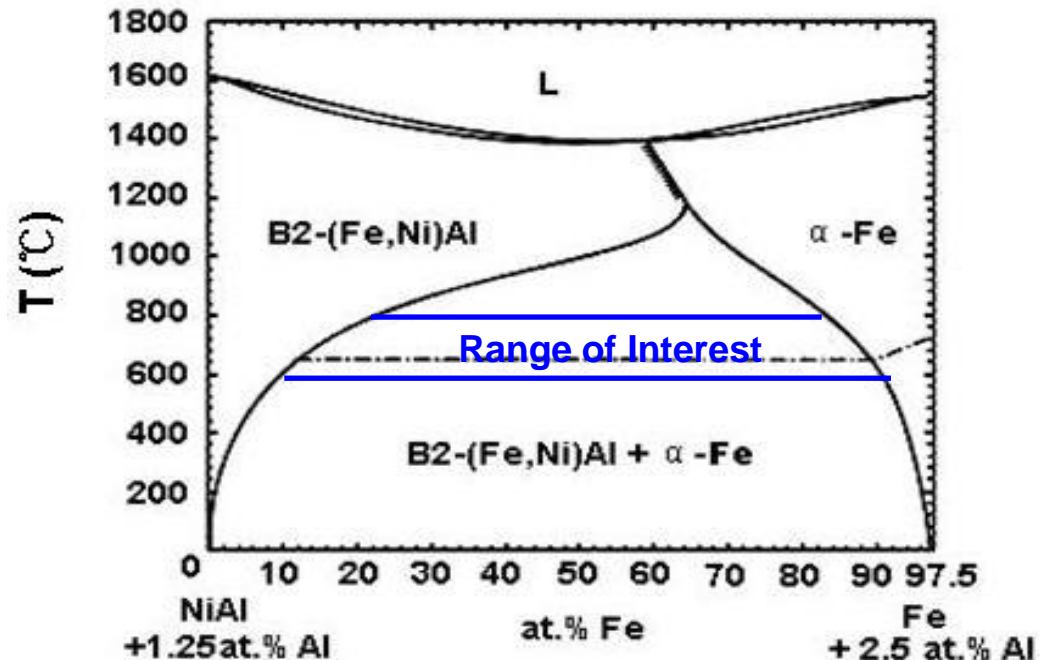
Ordered B2 (Fe, Ni)Al-type and ordered L2$_1$ Ni$_2$TiAl-type precipitates can form in a coherent-coplanar orientation, providing the possibility of achieving a Fe-based analogue to the Ni-based superalloys.

34

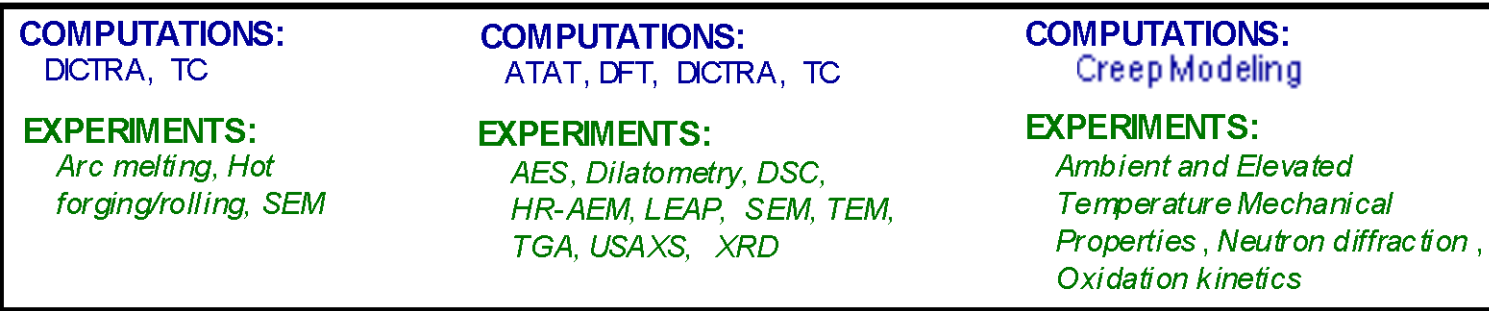# Ferritic Superalloys as a Materials System

PROCESSING   STRUCTURE   PROPERTIES

AGING

HOMOGENI-ZATION

HOT-ROLLING/HOT-FORGING

SOLIDIFICATION

DEOXIDATION, REMELTING

PRIMARY MELTING

MATRIX
BCC solid solution of Fe
Lattice parameter (Mo,Ta)
Solid solution hardening
Diffusivity/mobility (Hf,Ta,W,Zr)
Cleavage resistance (Al,Co,Ni)

MICROSEGREGATION
Inhomogeneity

STRENGTHENING PHASE(S)
$B2$ Based on NiAl and/or
$L2_1$ based on Ni_2TiAl
Lattice parameter
Misfit control
Minimize coarsening rate
Avoid TCP phases:
Laves, σ, μ

GRAIN BOUNDARY CHEMISTRY
Pinning/sliding resistance:
Borides, carbides

CREEP RESISTANCE
(1,033 K, 35 MPa)

CLEAVAGE RESIS-TANCE, DUCTILITY
(Room temperature)

OXIDATION, CORROSION RESISTANCE

PERFORMANCE

COMPUTATIONS:
DICTRA, TC

EXPERIMENTS:
Arc melting, Hot forging/rolling, SEM

COMPUTATIONS:
ATAT, DFT, DICTRA, TC

EXPERIMENTS:
AES, Dilatometry, DSC, HR-AEM, LEAP, SEM, TEM, TGA, USAXS, XRD

COMPUTATIONS:
Creep Modeling

EXPERIMENTS:
Ambient and Elevated Temperature Mechanical Properties, Neutron diffraction, Oxidation kinetics

TC: Thermo-Calc; DICTRA: DIffusion Controlled TRansformations; DFT: Density Functional Theory; ATAT: Alloy Theoretic Automated Toolkit; HR-AEM: High-Resolution Analytical Electron Microscope; LEAP: Local Electrode Atom Probe; SEM/TEM: Scanning/Transmission Electron Microscope; TGA: Themo-Gravimetric Analysis; XRD: X-ray Diffraction

1.1 Proposed Research

- Principal computational tools
    - Vienna Ab-initio Simulation Package (VASP): total energy and electronic structures
    - Alloy Theoretic Automated Toolkit (ATAT): cluster expansion (energy, lattice parameter, elastic properties of disordered solid solutions), Monte Carlo simulation (diffuse interface energy)
    - Thermo-Calc: multi-component, multi-phase equilibria
        - Predictive accuracy depends on the accuracy of database
    - DICTRA: multi-component, multi-phase diffusion
        - Predictive accuracy depends on the accuracy of database

- Hardware resources
    - QUEST cluster (NU)
    - TeraGrid resources
    - NERSC resources (Lawrence Berkeley National Laboratory)

1.1 Calculation of *B*2 -> *L*2$_1$ Ordering Energy

- A systematic study of ordering energy: *B*2 —> *L*2$_1$ in Ni-Al-Ti system
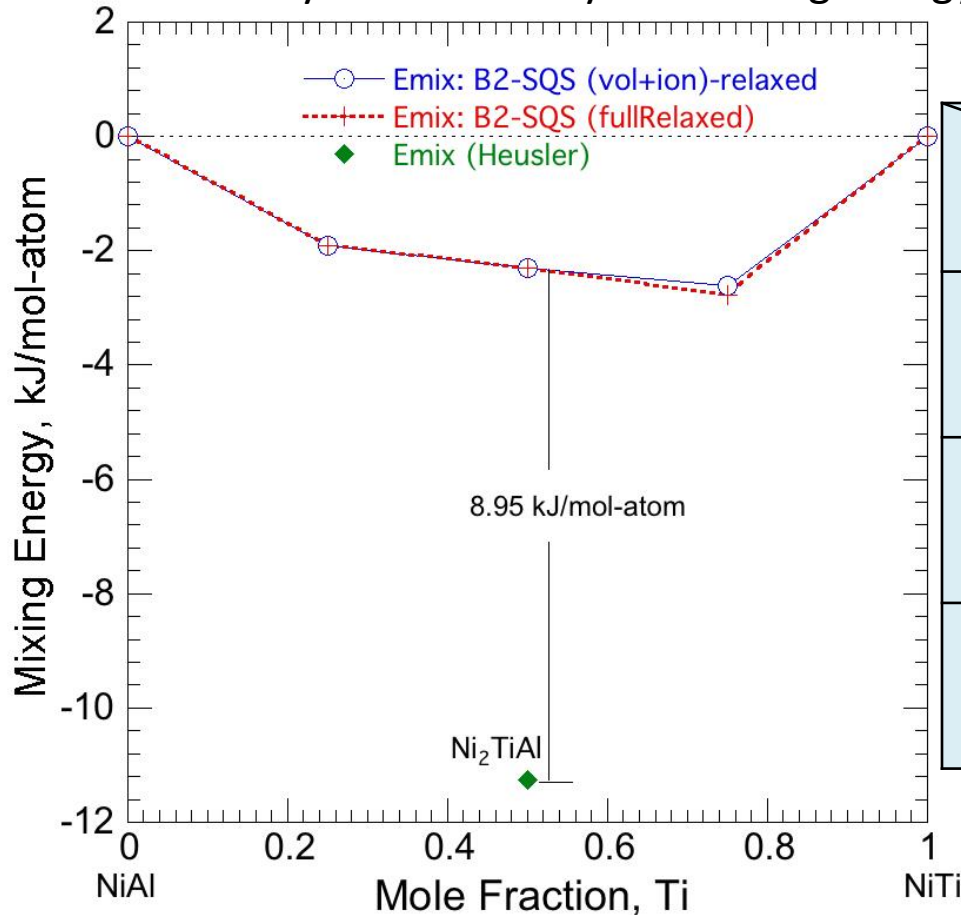
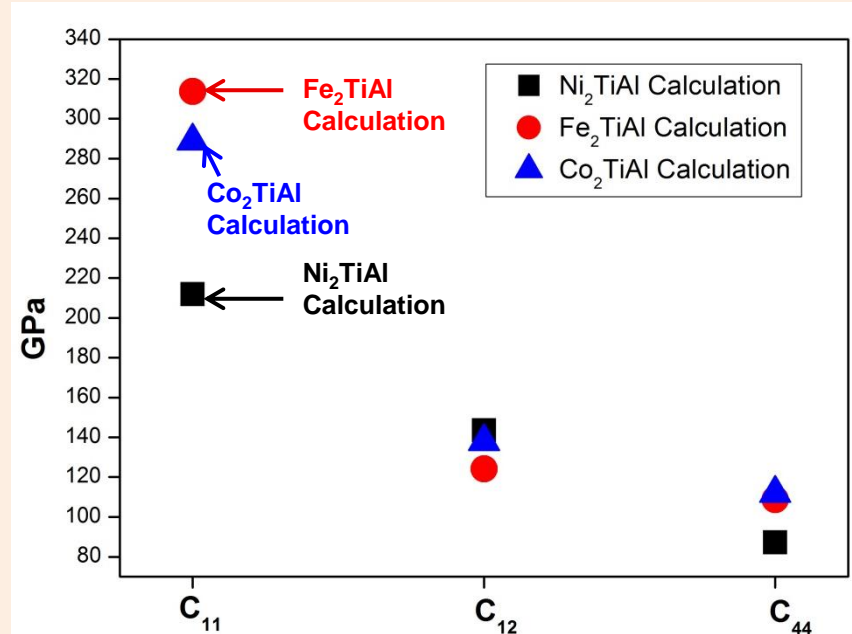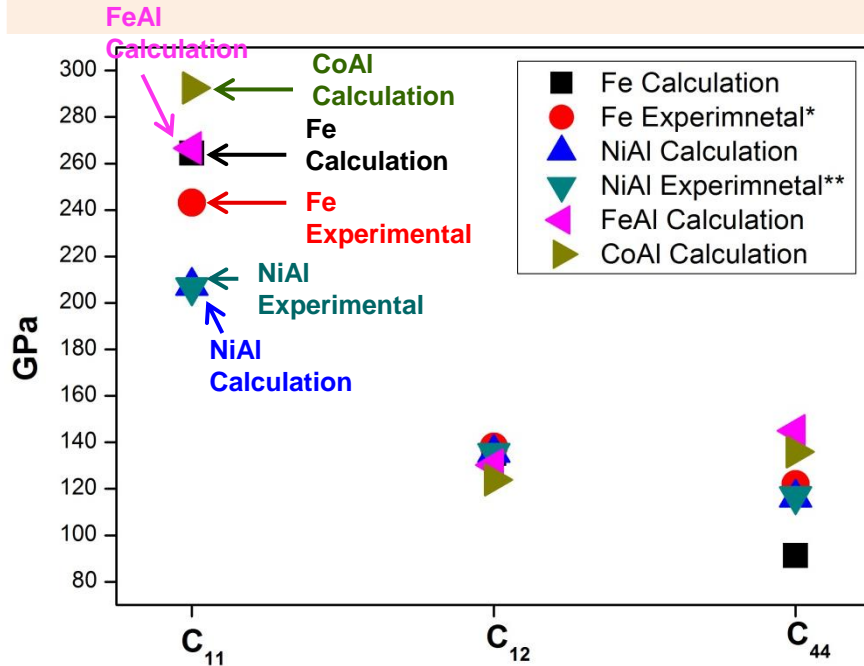| System \ Energy	Ordering Energy (kJ/mol-atom)
Ni-Al-Ti (NiAl → Ni$_2$TiAl)	8.95
Fe-Ti-Al (FeAl → Fe$_2$TiAl)	4.90
Co-Al-Ti (CoAl → Co$_2$TiAl)	7.09

- **Presently, calorimetry data is insufficient to derive *B*2 to *L*2$_1$ ordering energy in the Ni-Al-Ti system**
- **We have made use of Special Quasirandom Structure* supercell method followed by calculation of total energy from first-principles**
- ***B*2 to *L*2$_1$ ordering energy in the Ni-Al-Ti system: ≈ 9 kJ/mol-atom**

Ternary *B*2 Supercells were created (having Special Quasirandom Structure (SQS*)) along the section NiAl-NiTi

* A. Zunger, S-H. Wei, L.G. Ferreira and J.E. Berrnard *PRL*, 1990;**65**:353

Project Objectives

- Task 2: Thermodynamic and Kinetic Modeling of Multicomponent, Multiphase Alloys
    - This is a computation-intensive task. First-principles code along with state-of-the-art alloy theory tool have been utilized to carry out relevant computations. National facilities (XSEDE (or TeraGrid), supported/maintained by NSF, and NERSC, supported/maintained by DOE) were utilized in this task.

- A systematic study of ordering energy: $B2 \longrightarrow L2_1$ in Fe-Al-Ti system
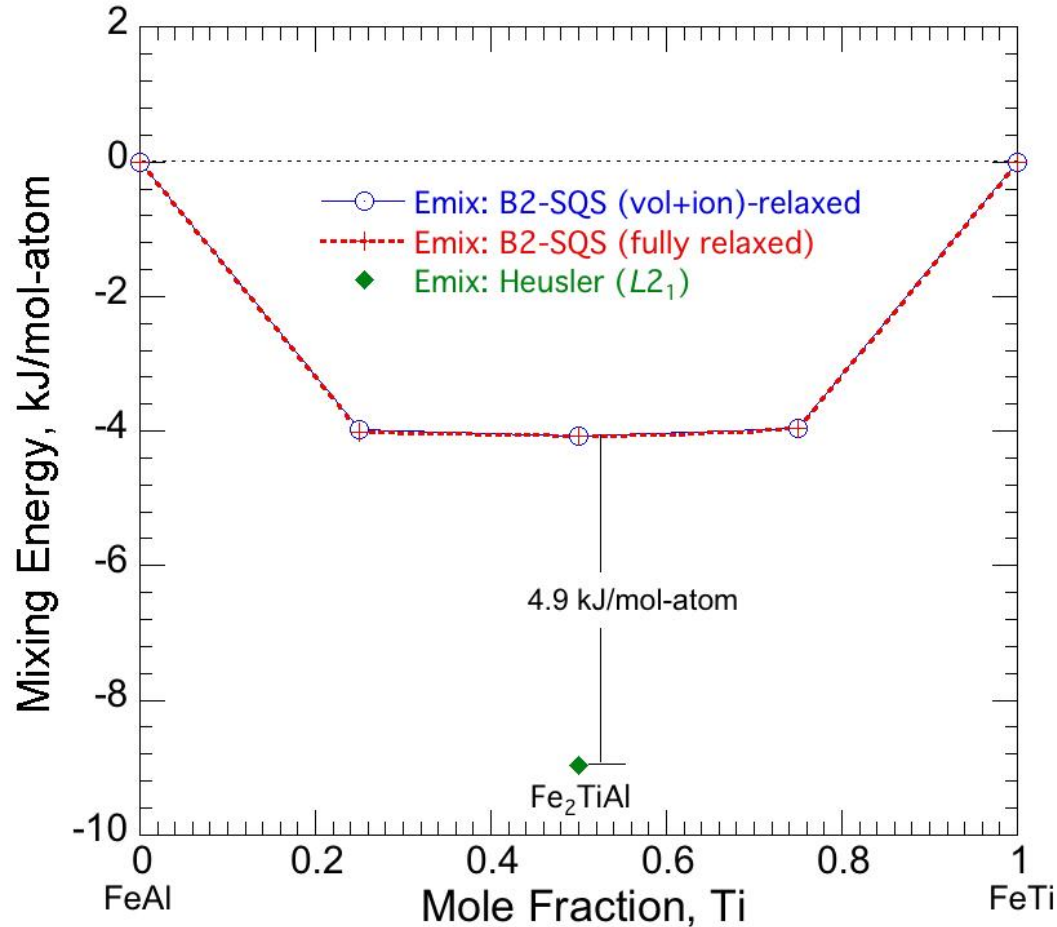
- **Presently, calorimetry data is insufficient to derive *B*2 to *L*2$_1$ ordering energy in the Fe-Al-Ti system**
- **We have made use of SQS* supercell method followed by calculation of total energy from first-principles**
- **B2 to L2$_1$ ordering energy in the Fe-Al-Ti system: ≈ 5 kJ/mol-atom**

Ternary *B*2 Supercells were created (having Special Quasirandom Structure (SQS*)) along the section FeAl-FeTi
* A. Zunger, S-H. Wei, L.G. Ferreira and J.E. Berrnard. PRL, 1990;65:353

1.1 Calculation of *B*2 -> *L*2$_1$ Ordering Energy

- A systematic study of ordering energy: $B2 \longrightarrow L2_1$ in Co-Al-Ti system
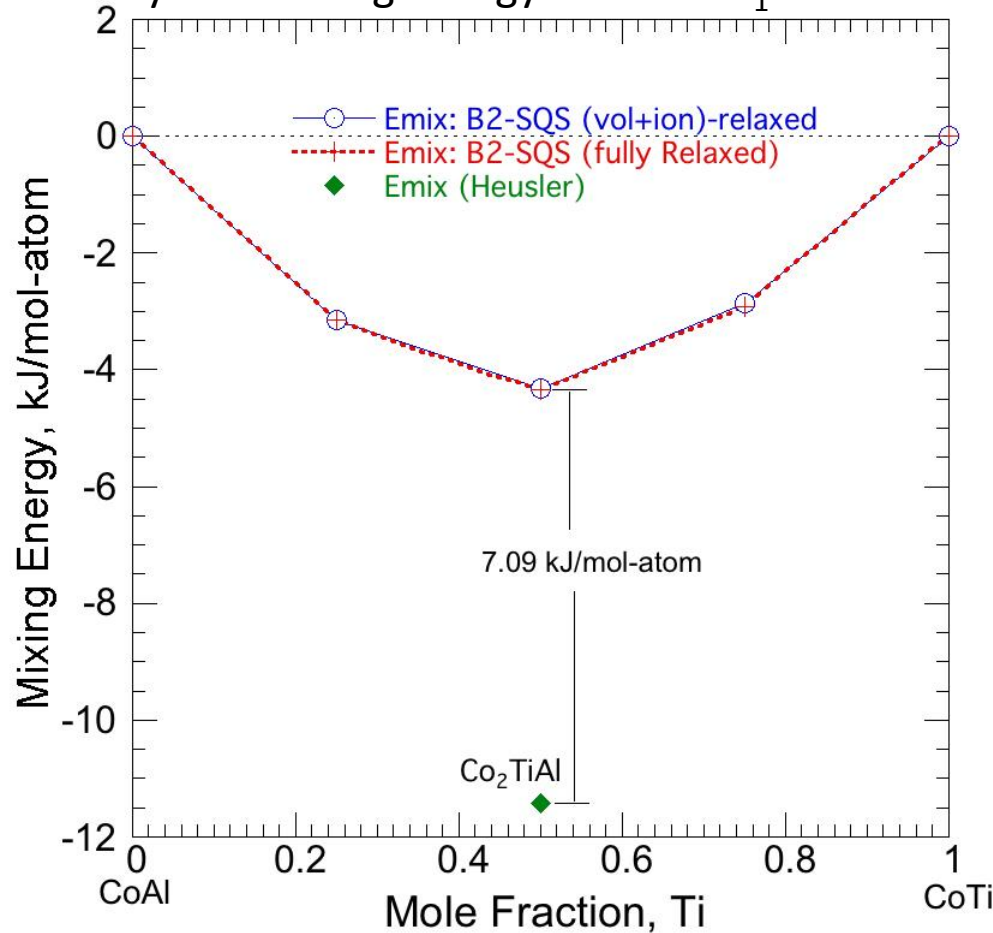
- **Presently, calorimetry data is insufficient to derive *B*2 to *L*2$_1$ ordering energy in the Co-Al-Ti system**
- **We have made use of SQS* supercell method followed by calculation of total energy from first-principles**
- **B2 to *L*2$_1$ ordering energy in the Co-Al-Ti system: ≈ 7.0 kJ/mol-atom**

Ternary *B*2 Supercells were created (having Special Quasirandom Structure (SQS*)) along the section CoAl-CoTi
   * A. Zunger, S-H. Wei, L.G. Ferreira and J.E. Berrnard. PRL, 1990;65:353

1.2 Calculation of Elastic Constants of Fe, *B2*, and *L2*$_1$ Phases

$$E(V,\{e_i\}) = E(V_0,0) - PV_0 \sum_{i=1}^{3} e_i + \frac{V_0}{2} \sum_{i=1}^{6} \sum_{j=1}^{6} C_{ij} e_i e_j + O[e_i^3]$$

FeAl Calculation

CoAl Calculation

Fe Calculation

Fe Experimental

NiAl Experimental

NiAl Calculation

Legend:
- ■ Fe Calculation
- ● Fe Experimnetal*
- ▲ NiAl Calculation
- ▼ NiAl Experimnetal**
- ◄ FeAl Calculation
- ► CoAl Calculation

Axis: GPa; C_{11}, C_{12}, C_{44}

Fe$_2$TiAl Calculation

Co$_2$TiAl Calculation

Ni$_2$TiAl Calculation

Legend:
- ■ Ni$_2$TiAl Calculation
- ● Fe$_2$TiAl Calculation
- ▲ Co$_2$TiAl Calculation

Axis: GPa; C_{11}, C_{12}, C_{44}

*At 4.2 K:
J.A. Rayne and B.S. Chandrasekhar, Phys. Rev., 1960, 120, 1658.
**50 at.% Ni and at 251 K:
T. Davenport, L. Zhou and J. Trivisonno, Phys. Rev. B, 1999, 59, 3421.

- C_{ij}s are obtained by first-principles method: total energy of the system as a function of deformation ($E(V,\{e_i\})$).
- A comparison of calculated C_{ij} of Fe and B2 phases were given previously in a quarterly progress report*.
- There is NO experimental C_{ij} data of Heusler phases, so calculations from first-principles is the only viable option.
- C_{ij} is needed to understand morphology of coherent precipitates and interfacial energy.

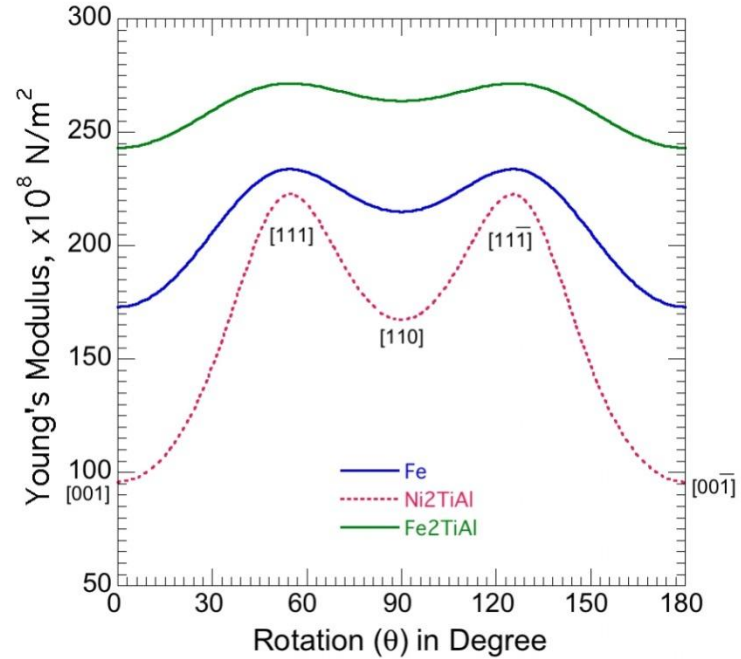* Report_DOE_DE-FE0005868_07292011.pdf

1.3 Orientation Dependence of Young's Modulus

$$\frac{1}{Y} = S_{11} - 2[(S_{11} - S_{12}) - \frac{1}{2}S_{44}](l_1^2 l_2^2 + l_2^2 l_3^2 + l_1^2 l_3^2)$$
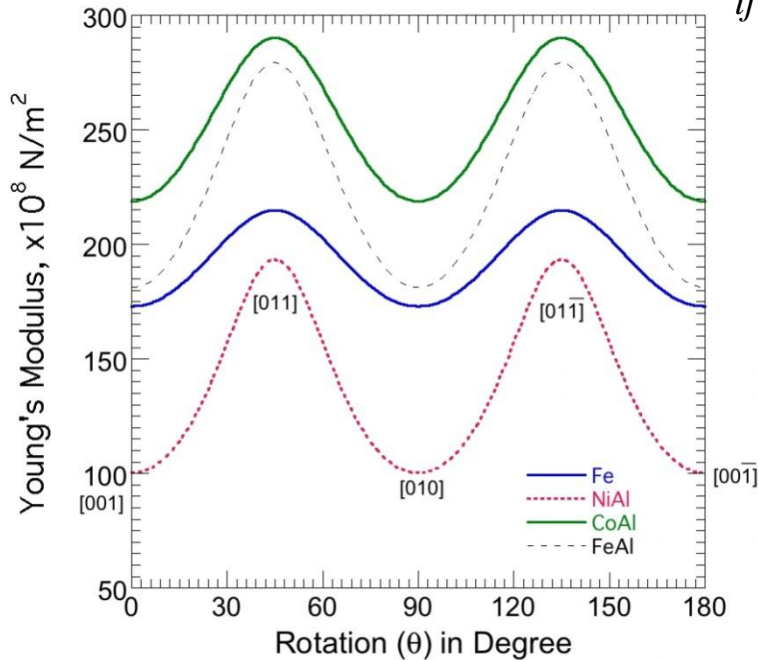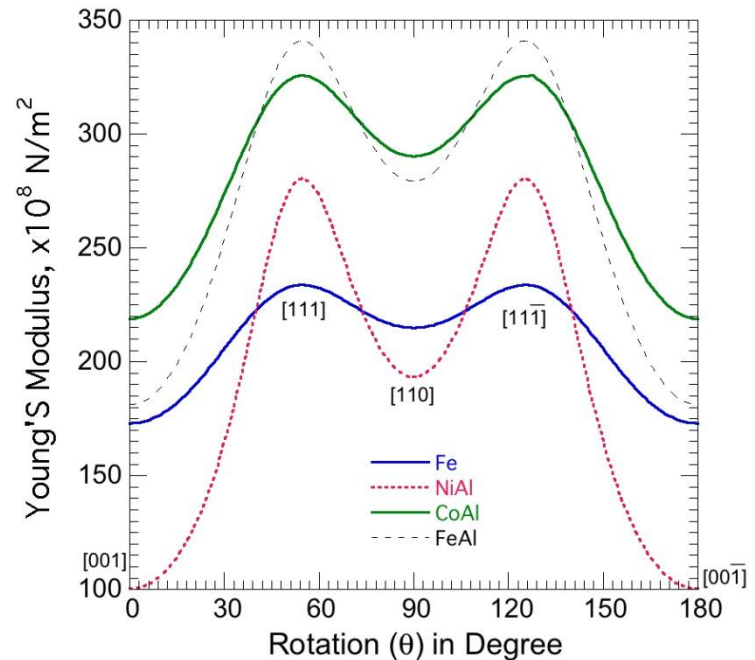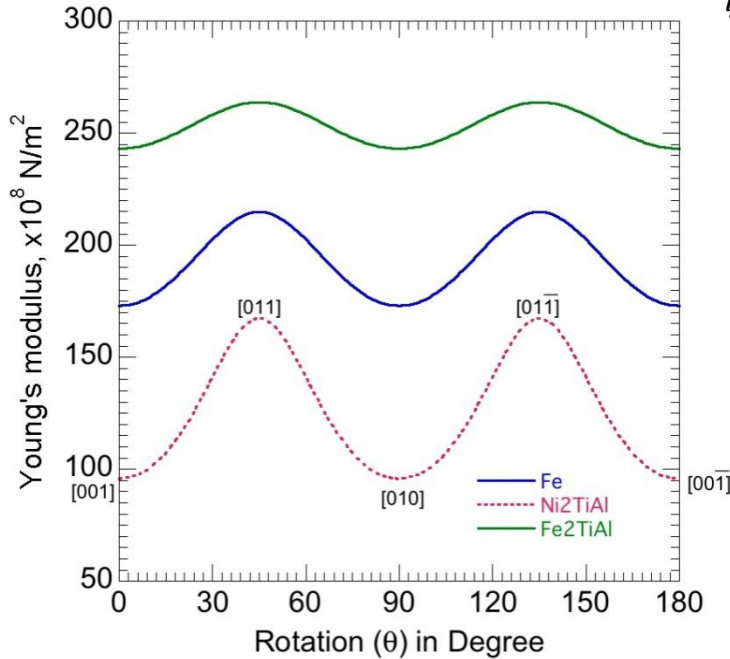
$$S_{ij} = C_{ij}^{-1}$$
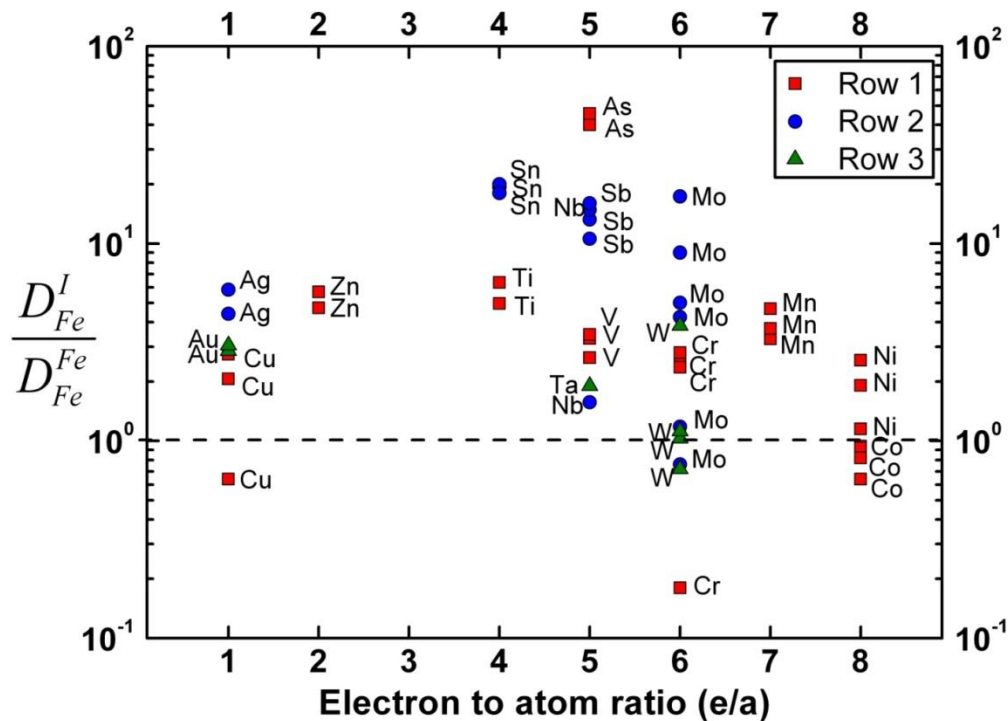

Tensile axis is rotated from $[001]$ **to** $[00\bar{1}]$ **around [100]**

Tensile axis is rotated from $[001]$ **to** $[00\bar{1}]$ **around** $[1\bar{1}0]$

- Orientation dependence of Young's modulus (Y) based on calculated C_{ij}*
- $B2$-NiAl is elastically softer in [001] direction than in [011] and [111] directions.
- NiAl is elastically softer than Fe
- Orientation dependence of Young's modulus is important to understand morphology (or shape) of coherent precipitates

* Discussed in Report_DOE_DE-FE0005868_07292011.pdf

$$\frac{1}{Y} = S_{11} - 2[(S_{11} - S_{12}) - \frac{1}{2}S_{44}](l_1^2 l_2^2 + l_2^2 l_3^2 + l_1^2 l_3^2)$$

$$S_{ij} = C_{ij}^{-1}$$

Tensile axis is rotated from $[001]$ to $[00\bar{1}]$ around [100]

Tensile axis is rotated from $[001]$ to $[00\bar{1}]$ around $[1\bar{1}0]$

- **Orientation dependence of Young's modulus (Y) based on calculated C_{ij}***
- **Ni_2TiAl is elastically softer in [001] direction than in [011] and [111] directions.**
- **Ni_2TiAl is elastically softer than Fe**
- **Orientation dependence of Young's modulus is important to understand morphology (or shape) of coherent precipitates**

* Discussed in Report_DOE_DE-FE0005868_07292011.pdf

Motivation

◆Data Lacking for Most 5d Solutes

◆Absence of Clear Slow Diffusers in Measured Data

S. Huang, D. L. Worthington, M. Asta, V. Ozolins, G. Ghosh, P. K. Liaw. Acta Materialia 58 (2010) 1982–1993
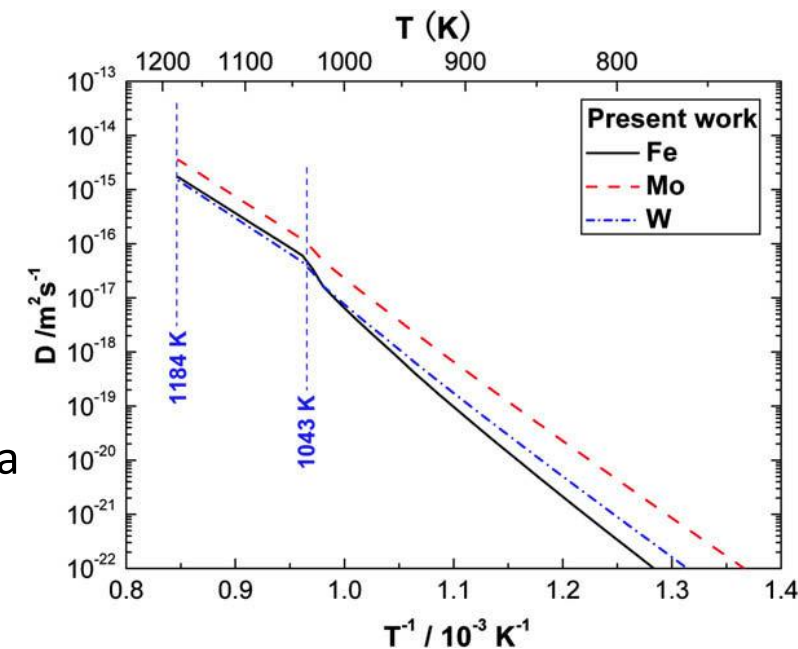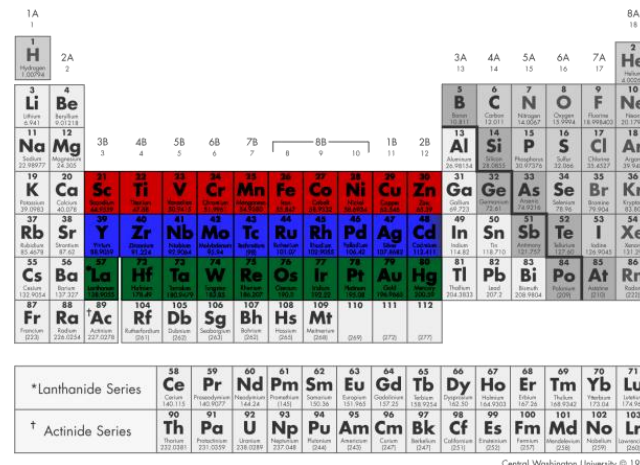
Magnetic Contributions
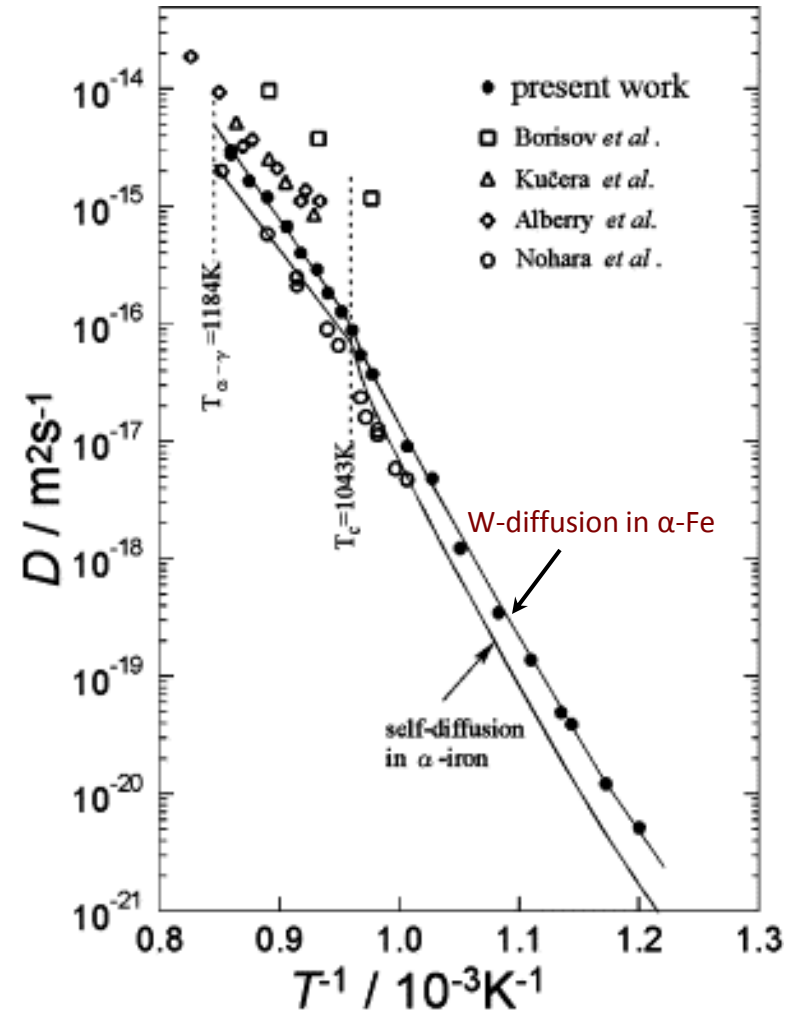
Magnetic Contribution in Ferromagnetic Phase

$$Q^F(T) = Q^P(1 + s(T)^2 \alpha)$$

$$s(T) = M(T) / M(0)$$

– α quantifies the influence of magnetic ordering on activation energy, Q

– α measured for relatively few solutes

S. Takemoto, H. Nitta, Y. Iijima, and Y. Yamazaki. *Phil Mag.,* 87, 1619 (2007).

Empirical Linear Relation: α and Induced Magnetization, ΔM_{12}

$$\Delta M_{12} = \sum_{i=1}^{8} \Delta m_i^{1st\ NN} + \sum_{j=1}^{6} \Delta m_j^{2nd\ NN}$$

S. Takemoto, H. Nitta, Y. Iijima, and Y. Yamazaki. *Phil Mag.,* 87, 1619 (2007).

– Calculate ΔM_{12} for solutes with known α

– Fit linear relationship

– Predict α for other solutes
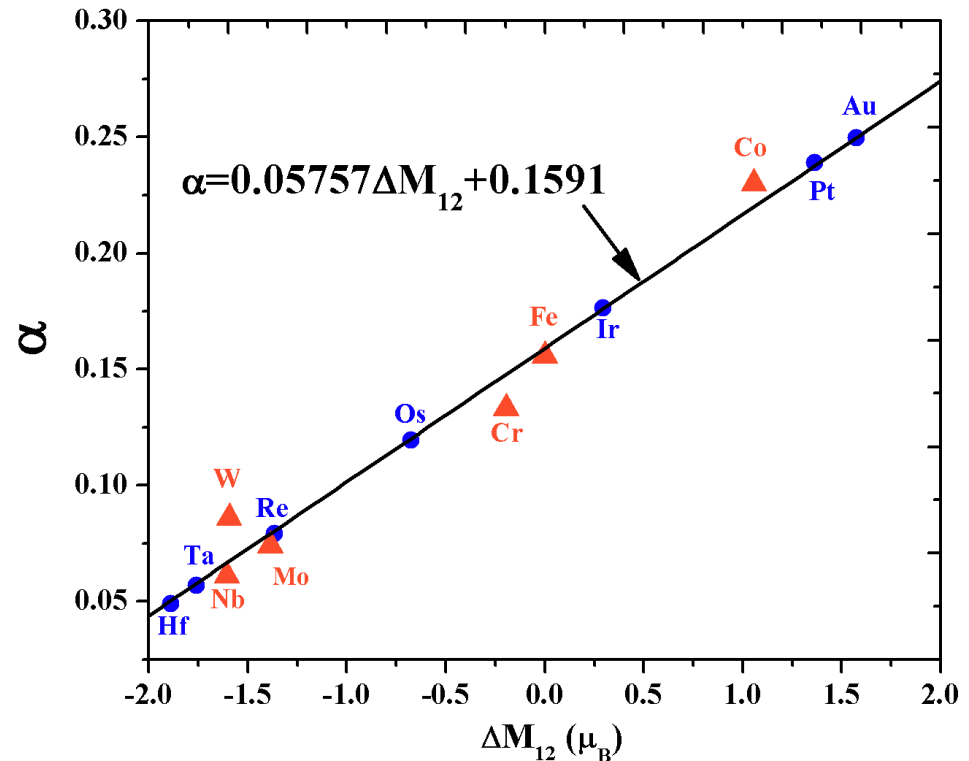
$\alpha = 0.05757 \Delta M_{12} + 0.1591$

Binding Energy

Migration Energy
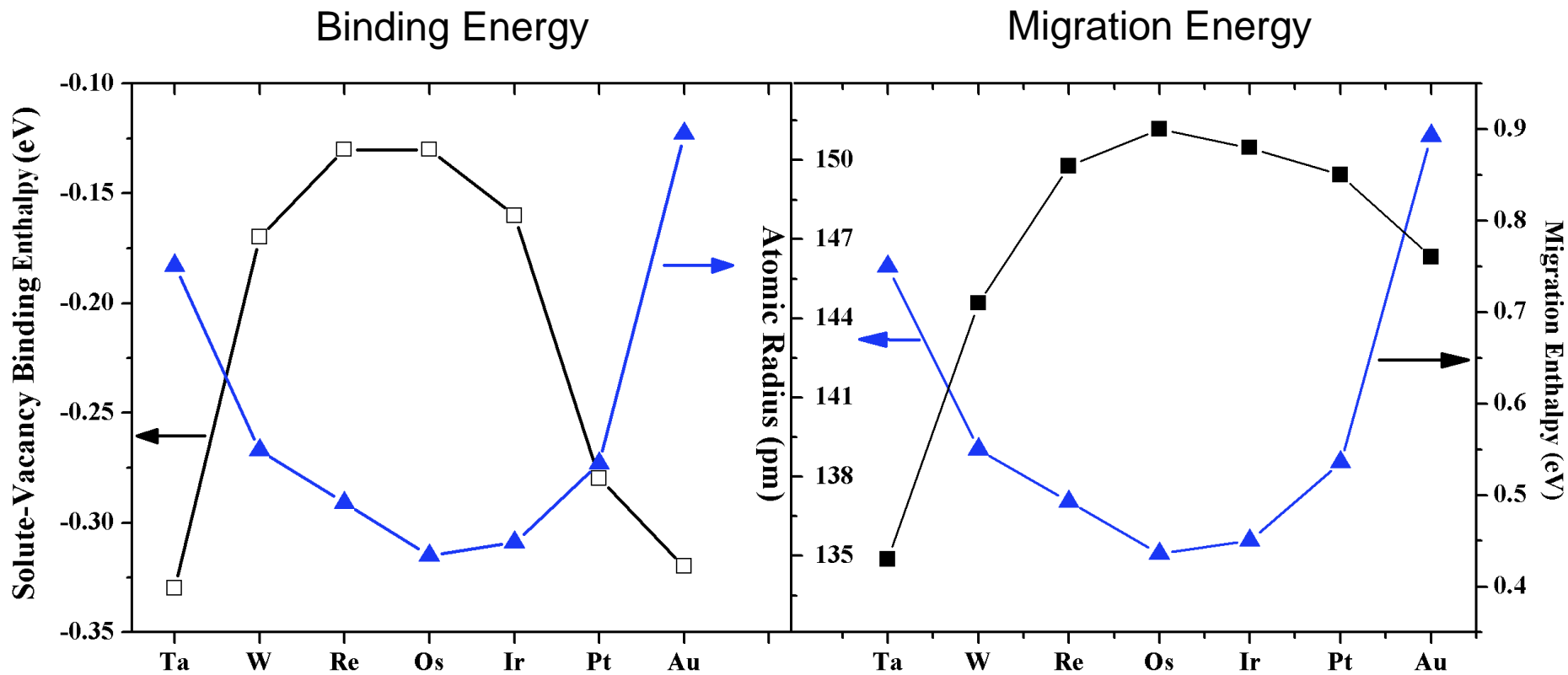
Smaller values of ΔH_b

Larger values of ΔH_m

Slower Impurity diffusivities

47

Heat-treated state after annealing at 700°C for 10 h: coherent interface

HRTEM $L2_1$-precipiate / bcc-Fe matrix along [001] zone axis
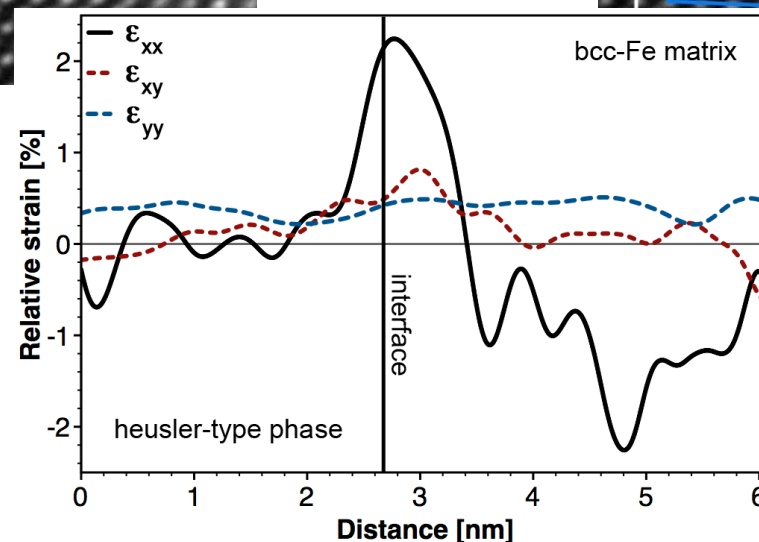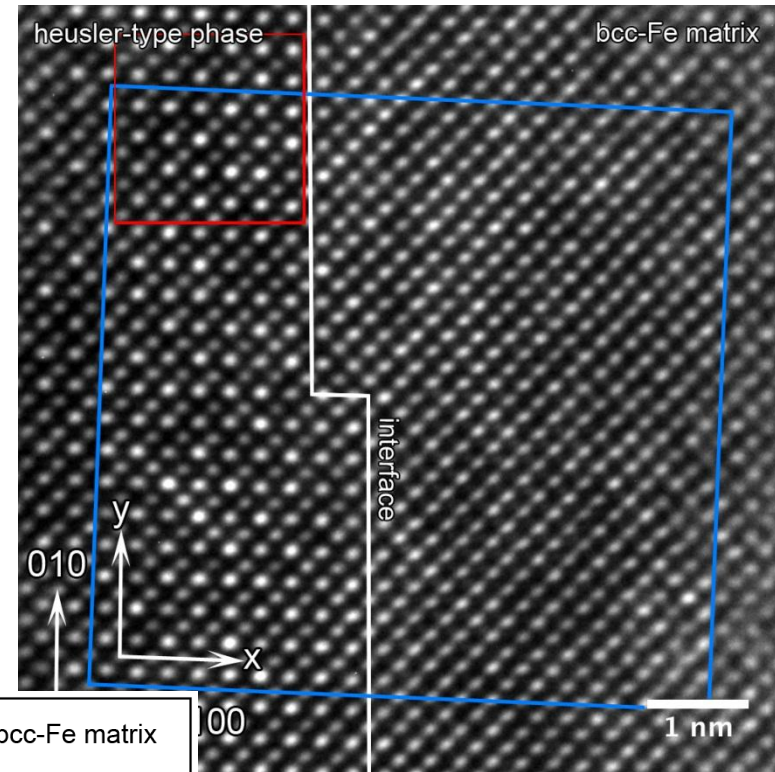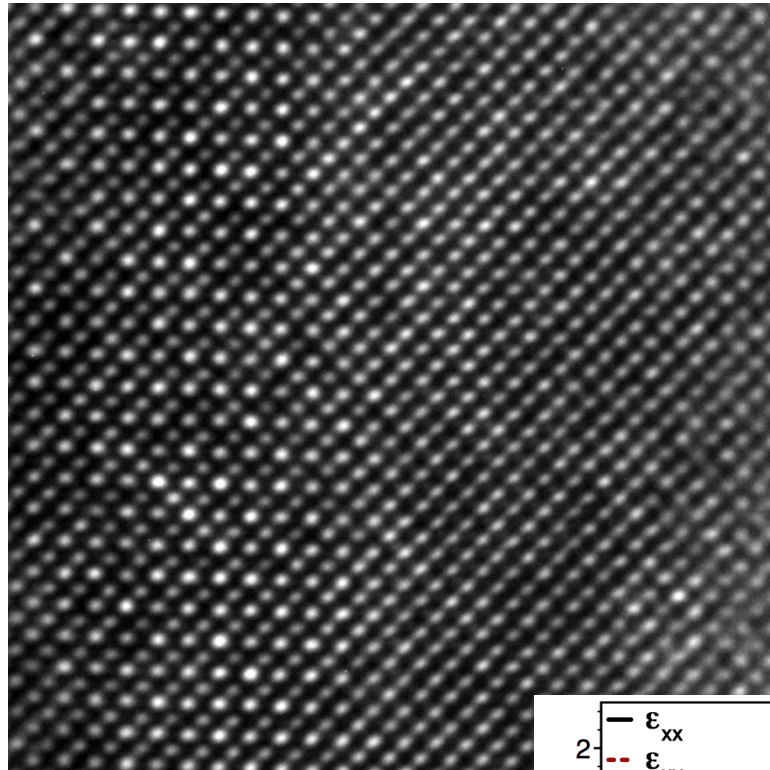
bcc-Fe matrix under compression with respect to L21-precipitate

Heat treated state after annealing at 700°C for 10 h:

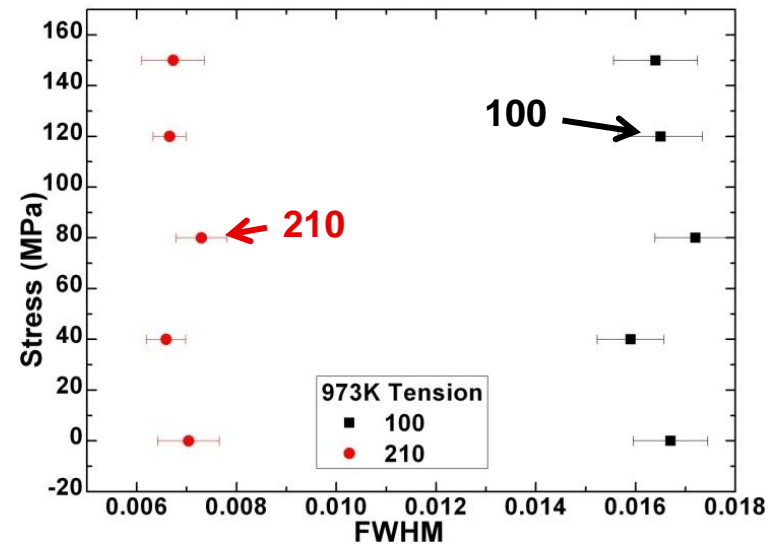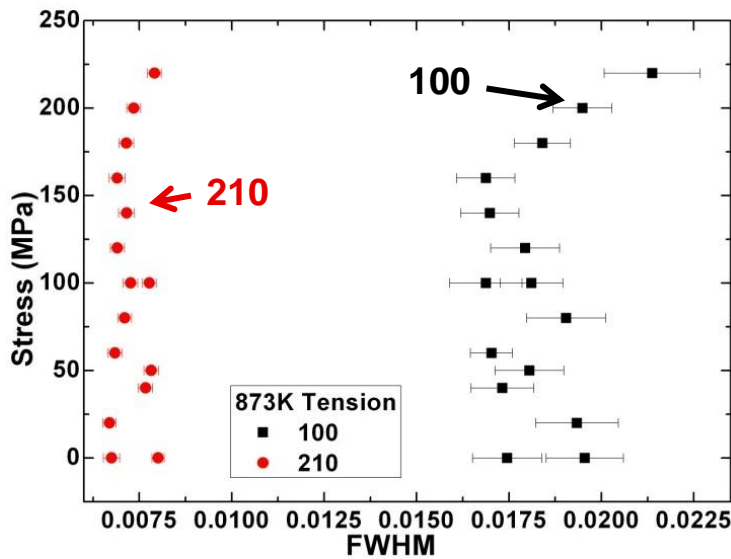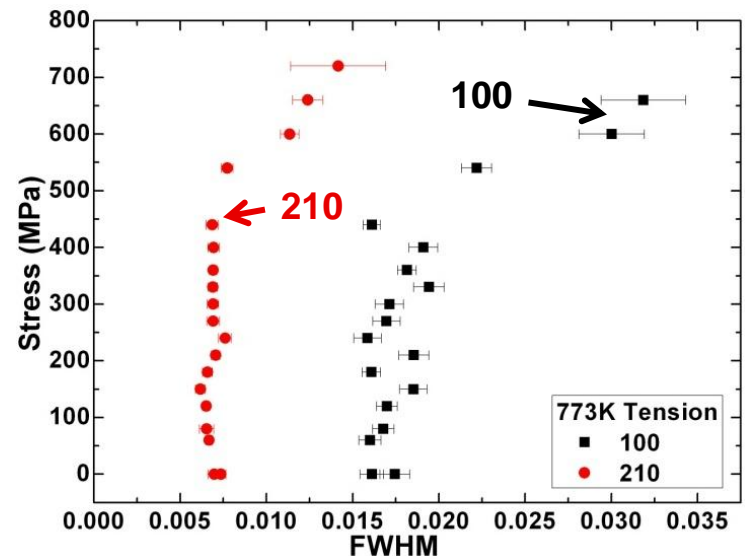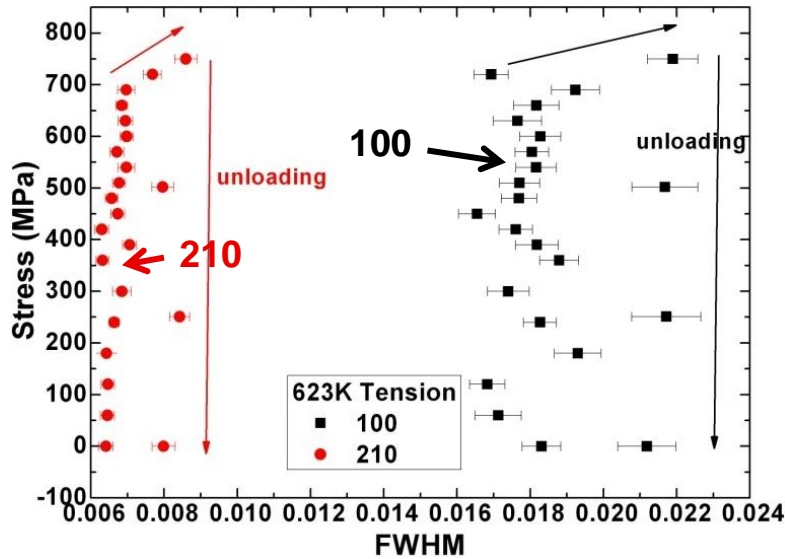Energy filtered TEM elemental maps of Ti, Ni, Fe and Cr
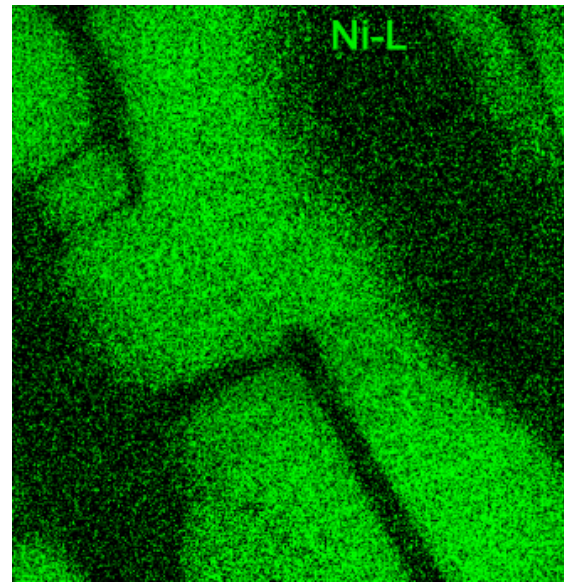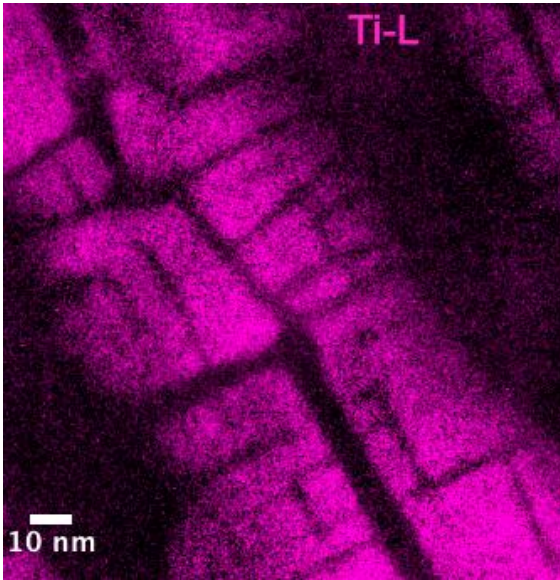
Depletion zones of Ti within $L2_1$-precipitates

B2-formation within $L2_1$-precipitates

49

- **Inhomogeneous dislocation-strain field causes peak broadening.**
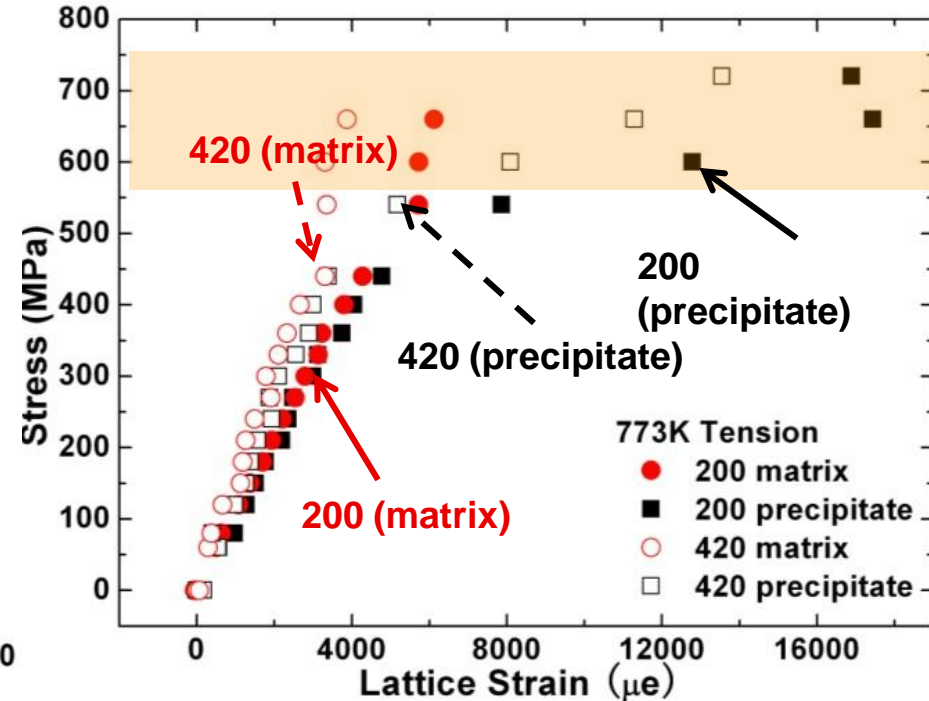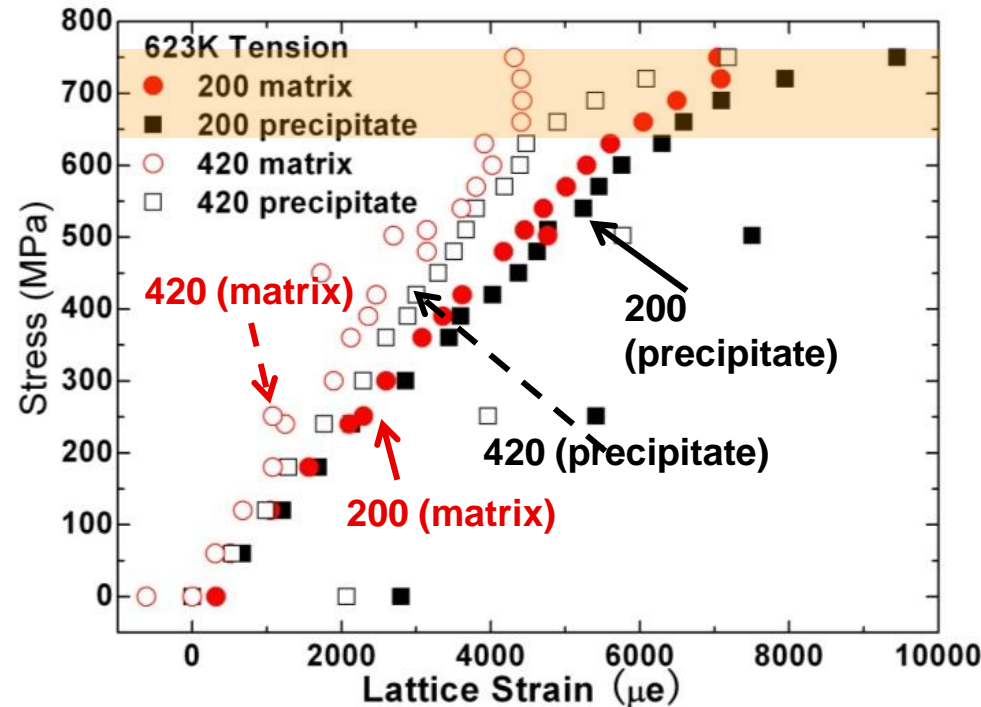
hkl-plane specific strain

- The onset of plastic deformation is marked by deviation from linear response
- Plastic anisotropy: plastic deformation occurs on certain preferential slip systems, and the sequence of grain yielding relies on Schmid factor
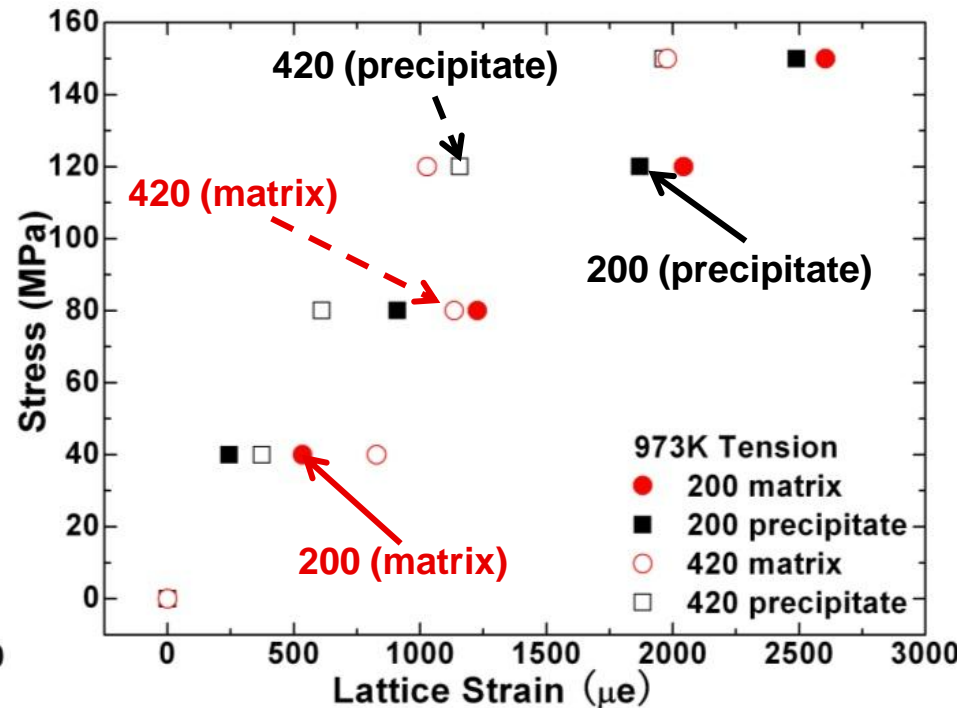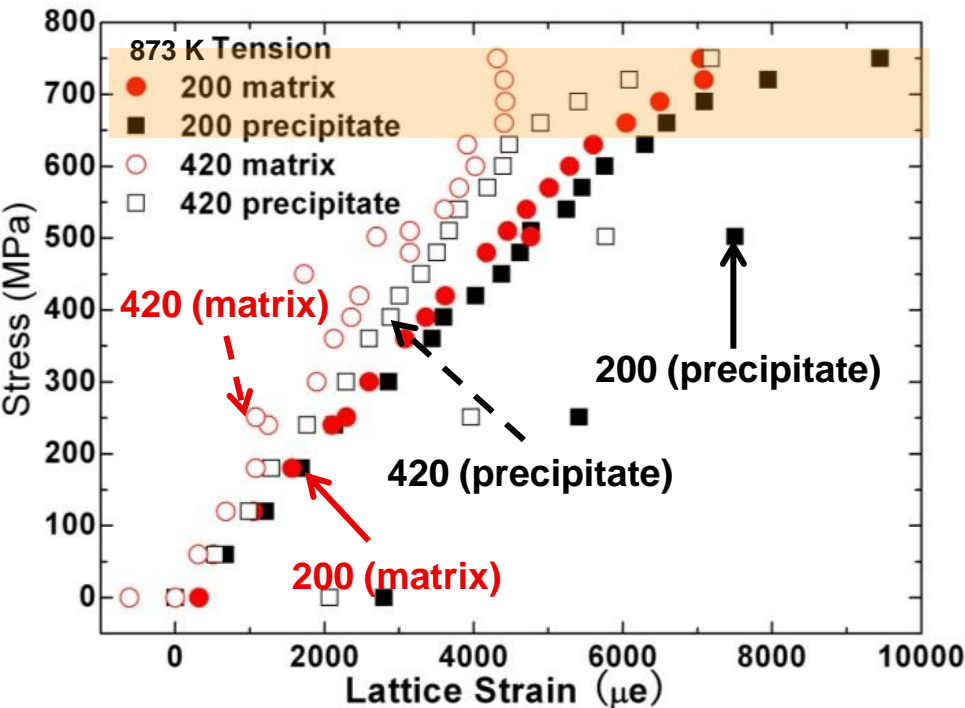- 110 and 420 oriented grains yield first with load transfer to 200 grains.

Local phase lattice strain

- **Interphase load transfer is superimposed on the intergranular load transfer.**

- **There is dramatic load transfer from matrix to precipitate phase at 773K, after yielding of most similarly oriented hkl grain families.**
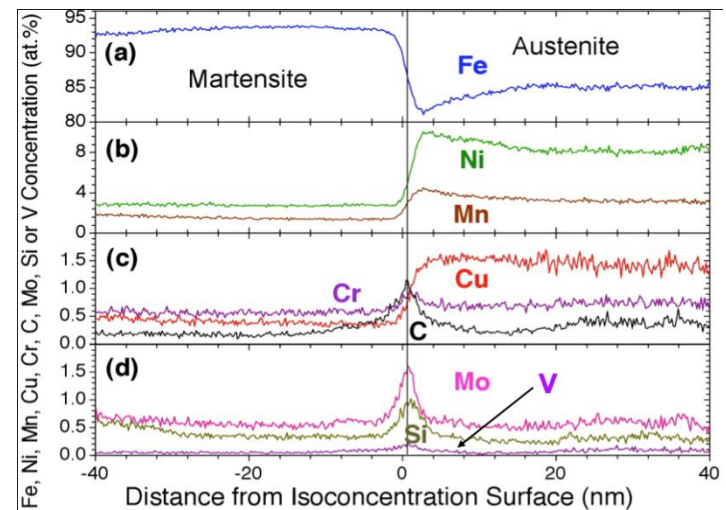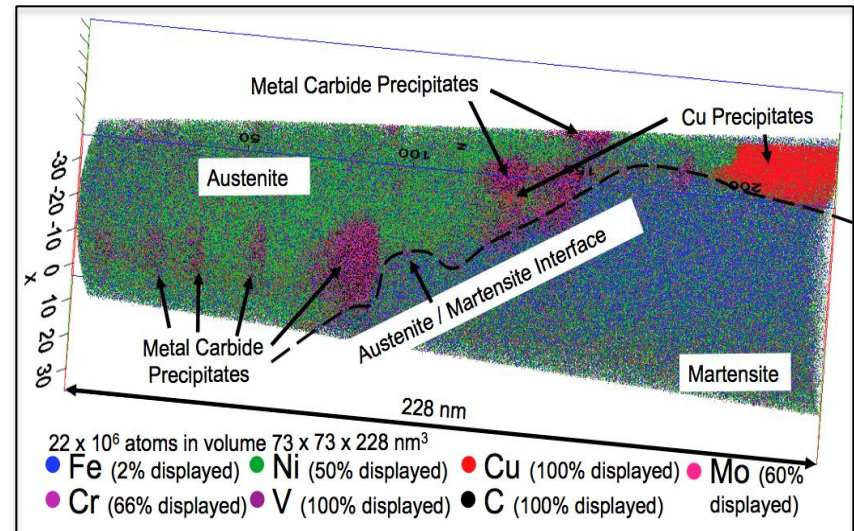
Local phase lattice strain

- At 973 K, macroscopic strain increases substantially at high stress levels due to creep. There is no obvious evidence of intergranular and interphase load transfer.
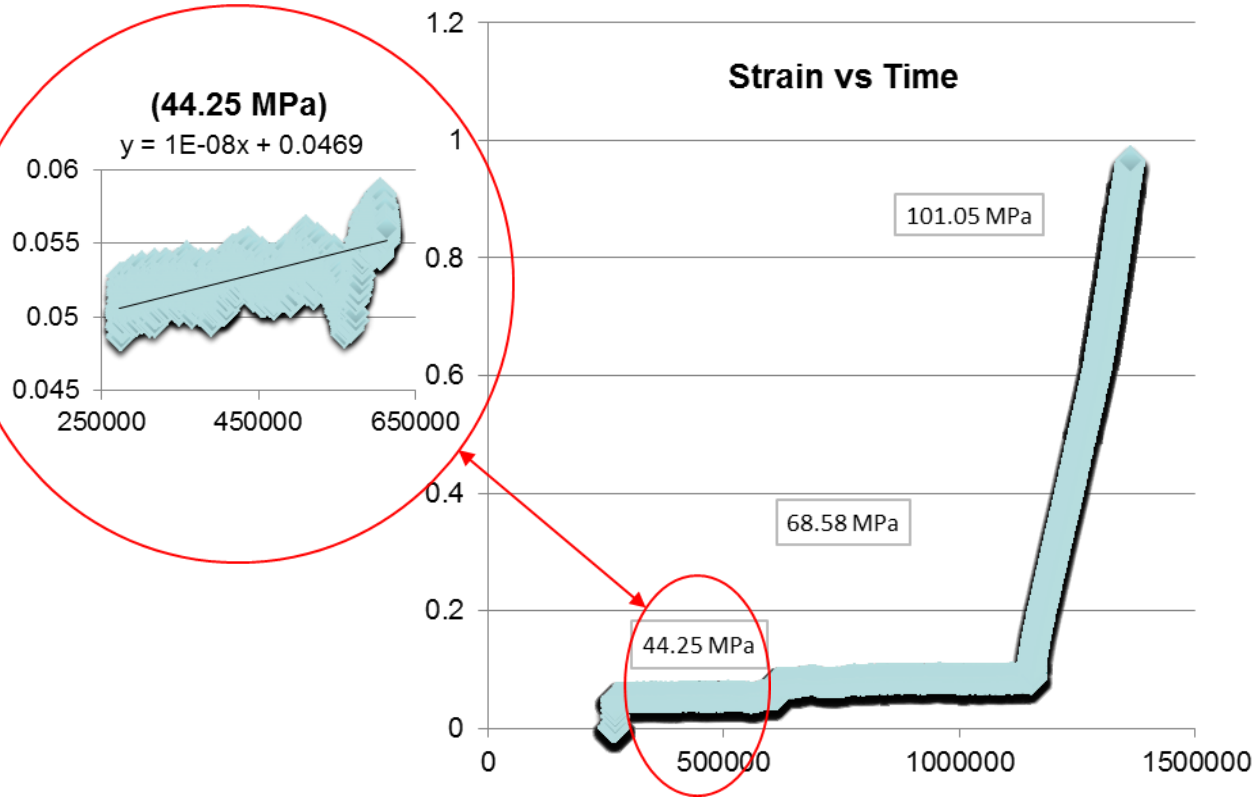
Local Electrode Atom Probe (LEAP) is a technique which yields a 3-D atom-by-atom tomographic reconstruction of a given material. In this case, a 4.5 wt% Ni steel.

What we learn from LEAP:

- Identify size, proximity and local composition of separate phases and precipitates present in the material.

- Examine interactions at the interface, such as an element-by-element analysis of the composition gradients present.

Metal Carbide Precipitates
Cu Precipitates
Austenite
Austenite / Martensite Interface
Metal Carbide Precipitates
Martensite
228 nm
22×10^6 atoms in volume $73 \times 73 \times 228$ nm^3
● Fe (2% displayed) ● Ni (50% displayed) ● Cu (100% displayed) ● Mo (60% displayed)
● Cr (66% displayed) ● V (100% displayed) ● C (100% displayed)

5.1 Creep Behavior

Sample 1 - Results

Stress (MPa)	Strain Rate (/s)
69	1e-08
101	4e-06
119	5e-05

Sample 2 - Results

Stress (MPa)	Strain Rate (/s)
73	9e-09
92	5e-09
109	8.9e-08

- Strain rates are calculated by isolating each individual stress level and taking the slope of that level
- Sample 1 results are vastly different from Sample 2 results
- Sample 2 results are more congruent with previous measurements

Spheres

s = 0.223
a = 0.522
N = 2

00:03.02

Cubes

s = 0.510
a = 0.308
N = 2

00:06.04
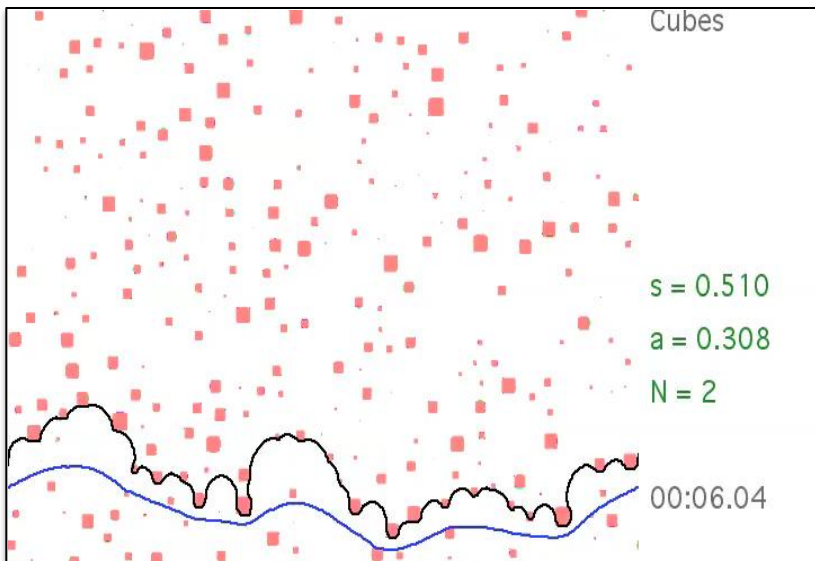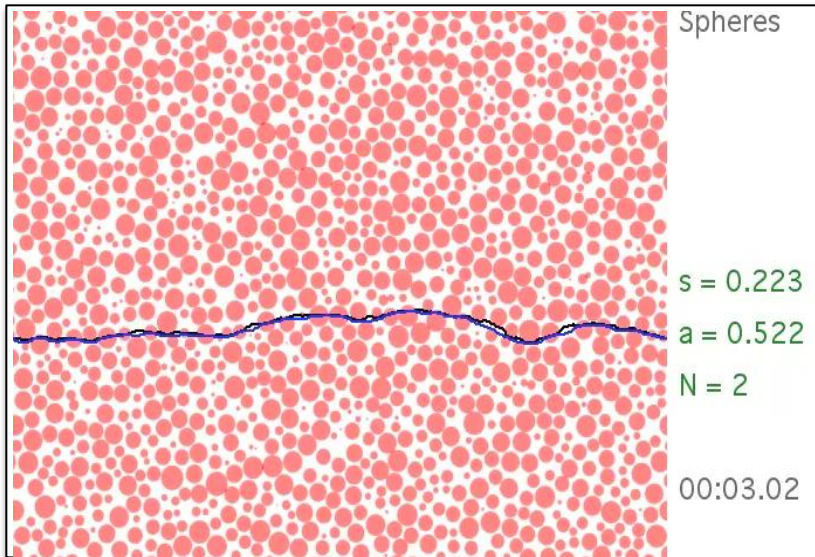
Accomplishments:

- Successfully achieved high volume fraction
- Achieved cuboidal precipitates

Future:

- Achieve high volume fraction and cuboidal precipitates simultaneously
- Establish various radii
- Simulate hierarchal precipitate structure
- Design optimal heat treatment

Images courtesy: Peter Bocchini, NU

Accomplishments:

- Successfully completed LEAP Training
- Become acquainted with electro-polishing technique
- LEAP blanks preparation (in progress)

Future:

- Prepare LEAP tips
- Atom Probe FBB8 samples
- Prepare and Atom Probe FBH8 samples
- Examine the interactions at the different phase interfaces in both materials
- Using datasets for Dislocation Dynamics Simulation

1. FBB8
   - Continue systematic study to verify previous creep results (from P. Liaw, UT)

   - Compression Creep
     a) Effect of stresses ranging from 40-200 MPa (stress exponent)
     b) Effect of temperature ranging from 600-700 ºC (activation energy)

   - Tension Creep
     a) Effect of stress 40-200 MPa (stress exponent)
     b) Effect of temperature 600-700 ºC (activation energy)
     c) Measure primary creep
     d) Measure tensile ductility + fracture time

2. Perform all of the same studies for the hierarchal FBH8 samples

Heat treated state after annealing at 700˚C for 10 h: composition measurements

TEM-EDS measurements reveal a composition of the bcc-Fe matrix of Fe$_{73}$Cr$_{19}$Al$_5$Ni$_3$ (at.%) and an overall composition of the *L2₁*-precipitates of Ni$_{33}$Fe$_{15}$Al$_{40}$Ti$_{10}$Cr$_1$ (at.%).

I$_{Ti}$/I$_{Ni}$-image

Relative quantification EFTEM:

$$\frac{N_A}{N_B} = \frac{I_A(b,\mathrm{D})}{I_B(b,\mathrm{D})}\frac{S_B(b,\mathrm{D})}{S_A(b,\mathrm{D})} = \frac{I_A(b,\mathrm{D})}{I_B(b,\mathrm{D})} \cdot k_{AB}$$

[Hofer, Ultramicroscopy 67 (1997), pp. 83-103]

Composition B2: (Ni$_{35}$Fe$_{15}$)(Al$_{46}$Ti$_4$)

Composition *L2₁*: (Ni$_{35}$Fe$_{15}$)Al$_{37}$Ti$_{13}$
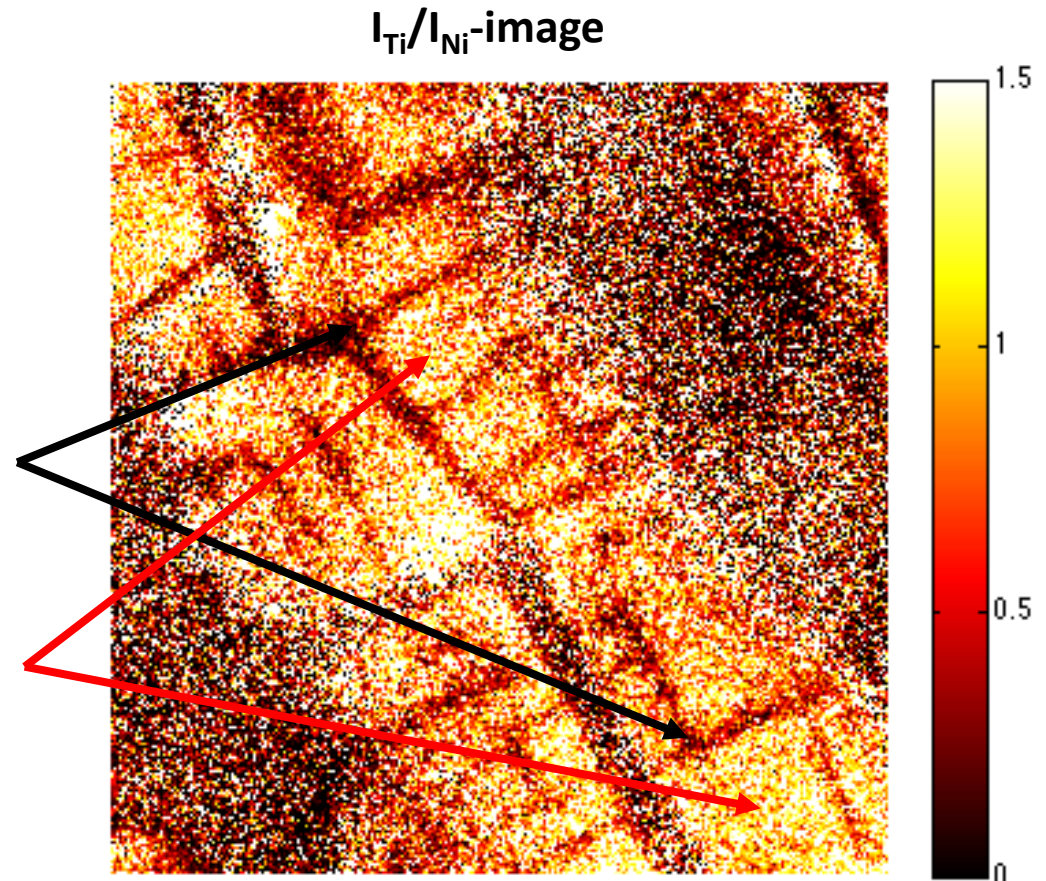
Conclusions

4. **Microstructural Characterization (Energy Filtered TEM, High Resolution TEM)**
   - $L2_1$-precipitates and a fine network of isotropic 100-type APBs within $L2_1$-precipitates are present in the as-quenched alloy.
   - B2-NiAl and residual 100-type APBs form within $L2_1$-precipitates in the heat-treated alloy.

5. **Preparation and Processing of Prototype Alloys**
   - Segregation in new-designed alloys with Ti contents may have significant impacts on mechanical properties of ferritic alloys. Further investigation will be performed regarding identifying segregation phases in the alloy system with the content of titanium.

6. **Neutron-Diffraction Measurements**
   - Deformation micromechanisms are evident from neutron diffraction measurements.
   - Below 773 K, the load transfer from the matrix to precipitates is effective in the plastic regime, following the dislocation slip mechanism.
   - Above 873 K, intergranular and interphase load transfer are not obvious in the plastic regime; the material undergoes power-law creep possibly due to grain boundary sliding or diffusional flow.
   - Crystal-plasticity finite-element simulation shows reasonably good agreement with neutron-diffraction measurements.
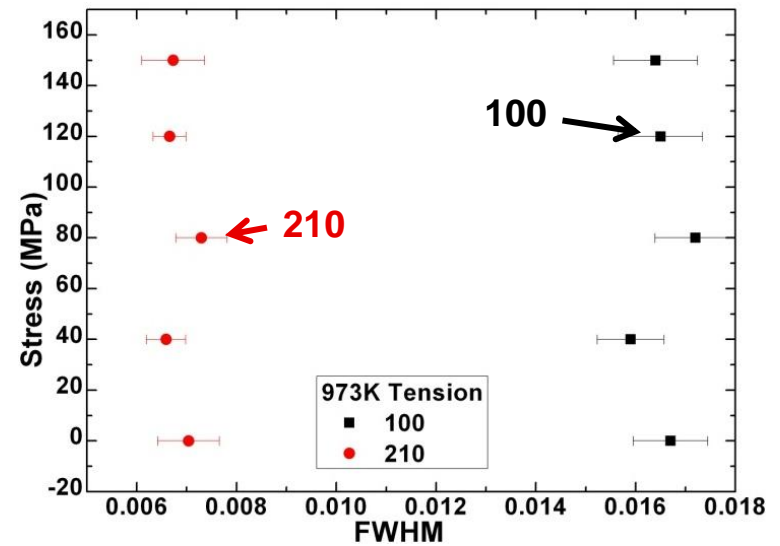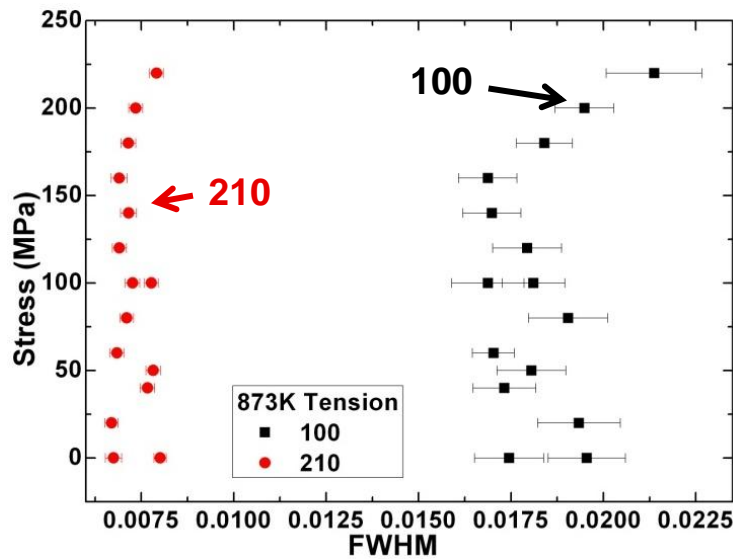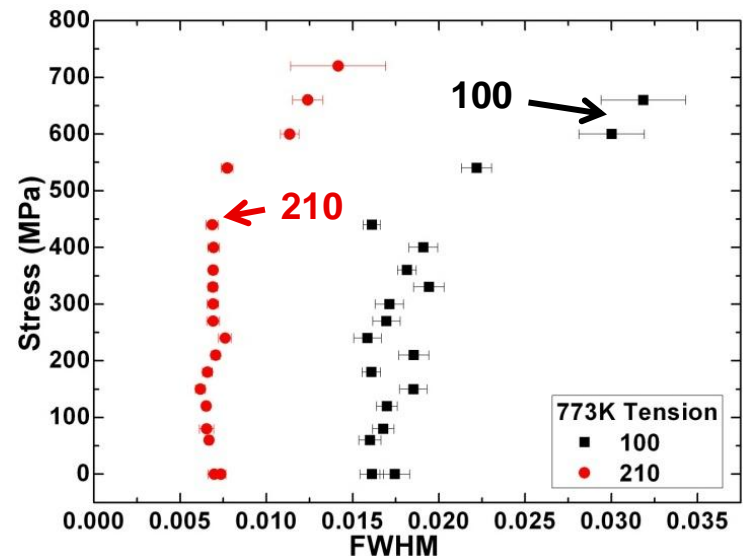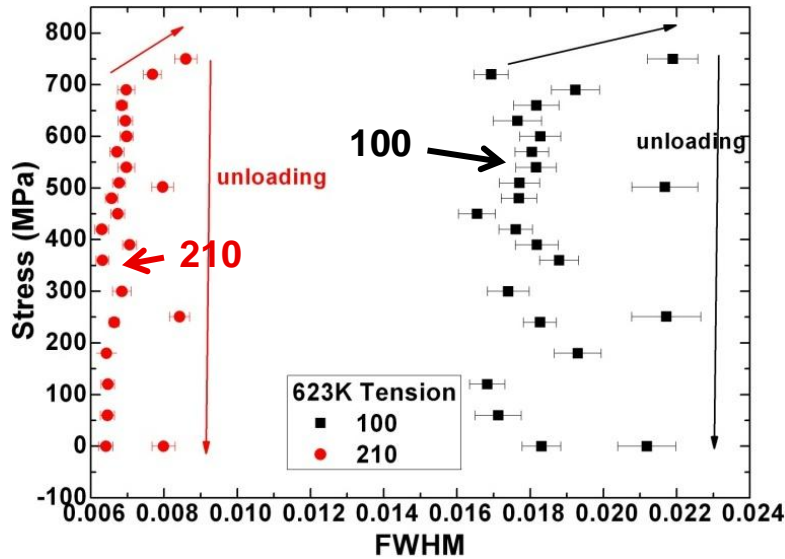
□ **Inhomogeneous dislocation-strain field causes peak broadening.**

6.5 Deformation Mechanisms

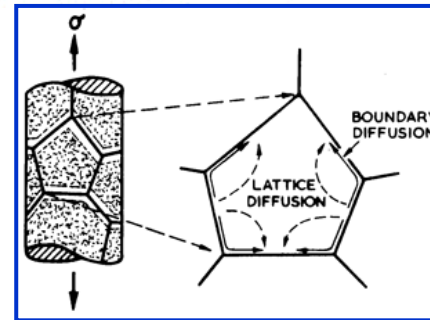**Temperature Increase, Stress Decrease** →

Dislocation Slip

✓ Lattice strain comparable to macroscopic strain

✓ Intergranular strain accumulated due to geometric grain boundary constraints and plastic anisotropy

✓ Effective interphase load transfer from matrix to precipitate

Power Law Creep

✓ Small lattice strain relative to macroscopic strain

✓ Low intergranular strain

✓ Plastic deformation is possibly assisted by grain boundary sliding or diffusional flow

✓ No interphase load transfer - interface diffusional flow

[1] Frost HJ, Ashby MF. Deformation Mechanism Maps: the Plasticity and Creep of Metals and Ceramics, Chapter 8. Oxford, UK: Pergamon Press, 1982.

6.5 Deformation Mechanisms

Temperature Increase, Stress Decrease →
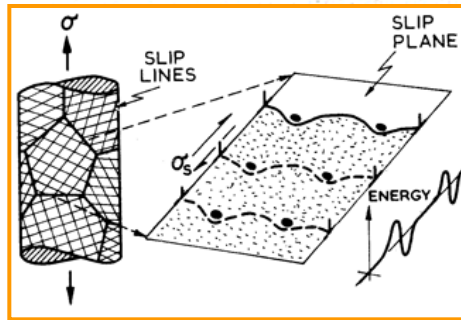
Dislocation Slip

- ✓ Lattice strain comparable to macroscopic strain
- ✓ Intergranular strain accumulated due to geometric grain boundary constraints and plastic anisotropy
- ✓ Effective interphase load transfer from matrix to precipitate
- ✓ Precipitate peak broadening

Power Law Creep

- ✓ Small lattice strain relative to macroscopic strain
- ✓ Low intergranular strain
- ✓ Plastic deformation is possibly assisted by grain boundary sliding or diffusional flow
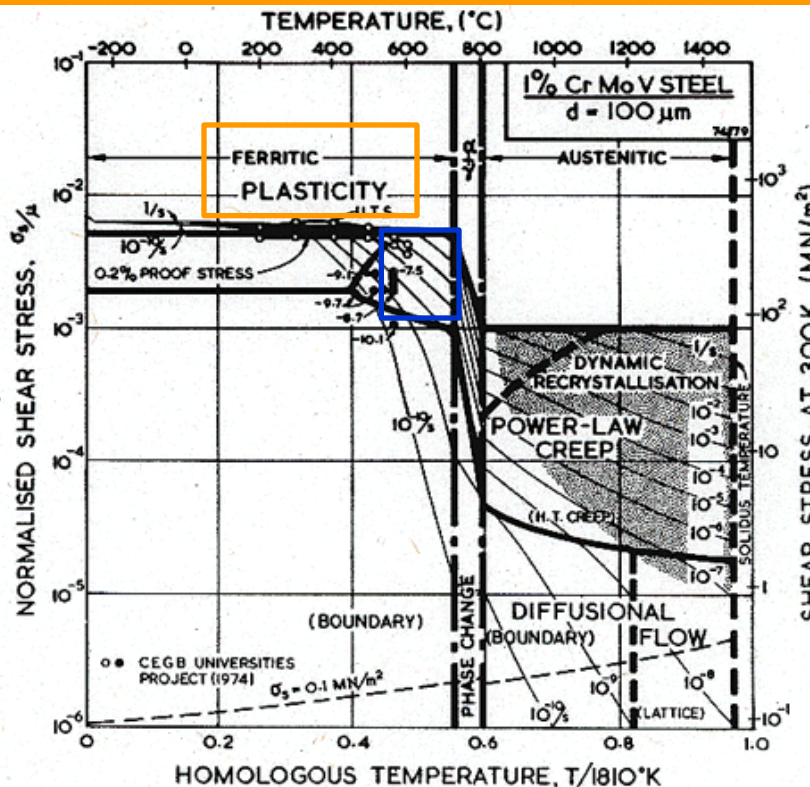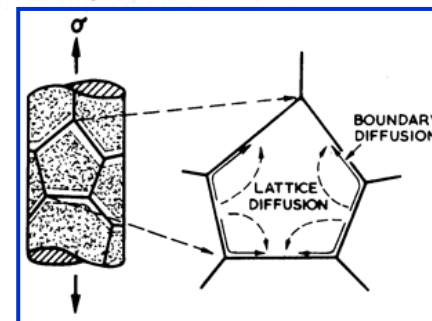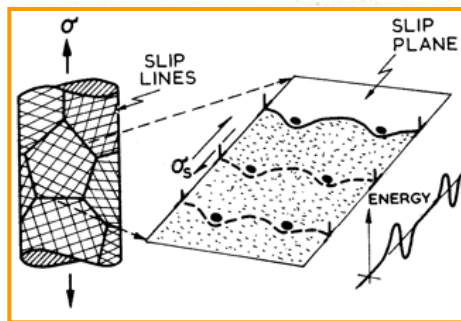- ✓ No interphase load transfer - interface diffusional flow
- ✓ No precipitate peak broadening

[1] Frost HJ, Ashby MF. Deformation Mechanism Maps: the Plasticity and Creep of Metals and Ceramics, Chapter 8. Oxford, UK: Pergamon Press, 1982.

Conclusions

1. **Ordering Energy Calculations**
   - To understand alloy thermodynamics, we have calculated energy for B2 to $L2_1$ ordering in ternary alloys.
   - Experimental calorimetry data is insufficient to estimate/derive such ordering energy in ternary alloys. So, calculations from first-principles is the only viable option.

2. **Calculations of Elastic Constants**
   - Single-crystal elastic constants (Cij) of Fe and relevant B2 phases are calculated from first-principles. They show a good agreement with experimental data, where available.
   - There is no experimental Cij data of Heusler phases. Thus, calculations from first-principles are the only viable option.

3. **Kinetic Modeling of Multicomponent Alloys**
   - First-principles methods have been conducted to predict diffusivities and interdiffusion coefficients in dilute body-centered cubic (bcc)-Fe solutions and binary alloys.

Conclusions (Cont'd)

4. **Microstructural Characterization (Energy Filtered TEM, High Resolution TEM)**
   - $L2_1$-precipitates and a fine network of isotropic 100-type APBs within $L2_1$-precipitates are present in the as-quenched alloy.
   - B2-NiAl and residual 100-type APBs form within $L2_1$-precipitates in the heat-treated alloy.

5. **Preparation and Processing of Prototype Alloys**
   - Segregation in new-designed alloys with Ti contents may have significant impacts on mechanical properties of ferritic alloys.

6. **Neutron-Diffraction Measurements**
   - Below 773 K, intergranular and interphase load transfer are observed in the plastic regime, following the dislocation slip mechanism.
   - Above 873 K, intergranular and interphase load transfer are not obvious in the plastic regime; the material undergoes power-law creep possibly due to grain boundary sliding or diffusional flow.
   - Crystal-plasticity finite-element simulations show reasonably good agreement with neutron-diffraction measurements.

6.2 Tension at 623 and 773 K – hkl plane-specific strain
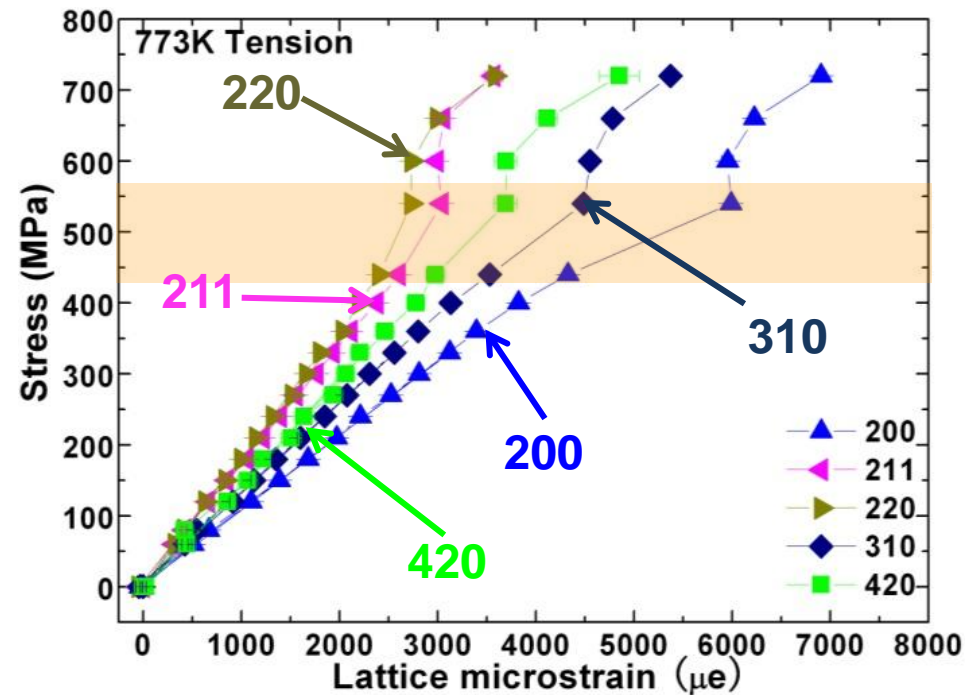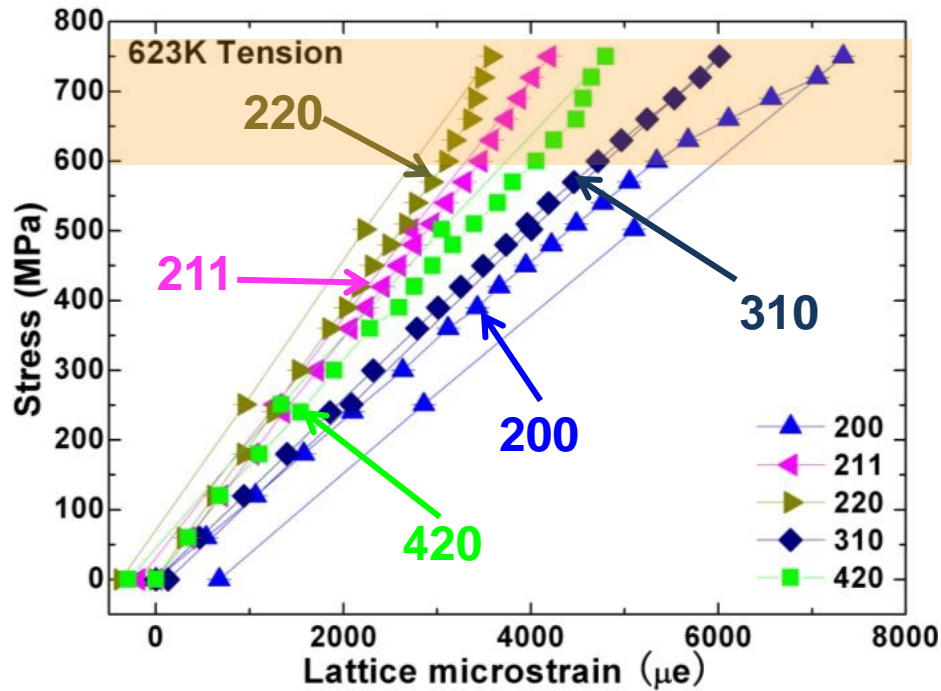
hkl plane-specific strain

- The onset of plastic deformation is marked by deviation from linear response
- Plastic anisotropy: plastic deformation occurs on certain preferential slip systems, and the sequence of grain yielding relies on Schmid factor
- 110 and 420 oriented grains yield first with load transfer to 200 grains.

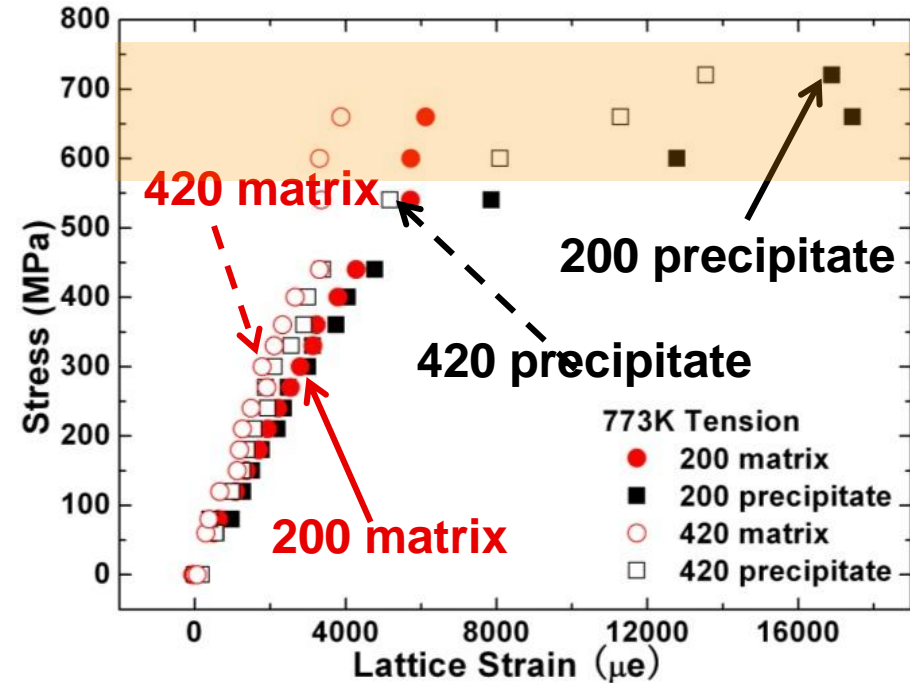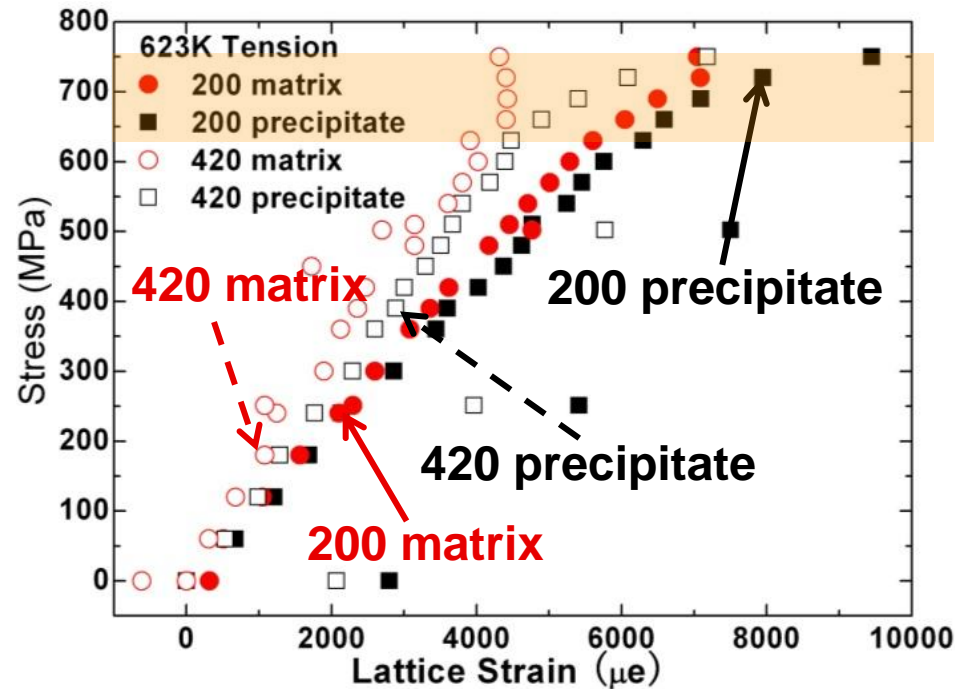# 6.2 Tension at 873 and 973 K – hkl plane-specific strain
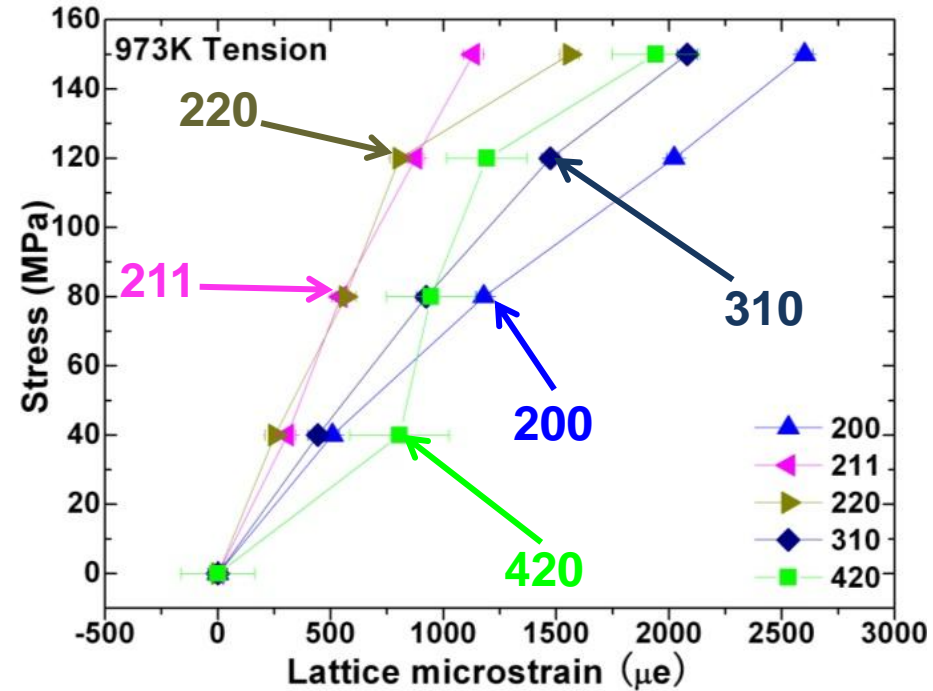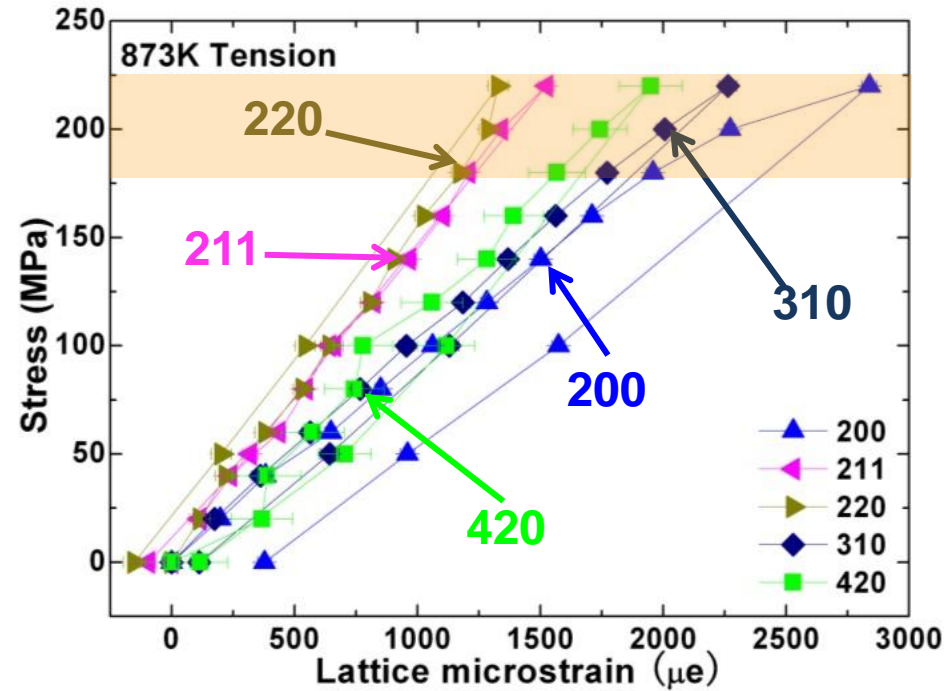
hkl plane-specific strain

- At 973 K, macroscopic strain increases substantially at high stress levels due to creep. There is no obvious evidence of intergranular and interphase load transfer.
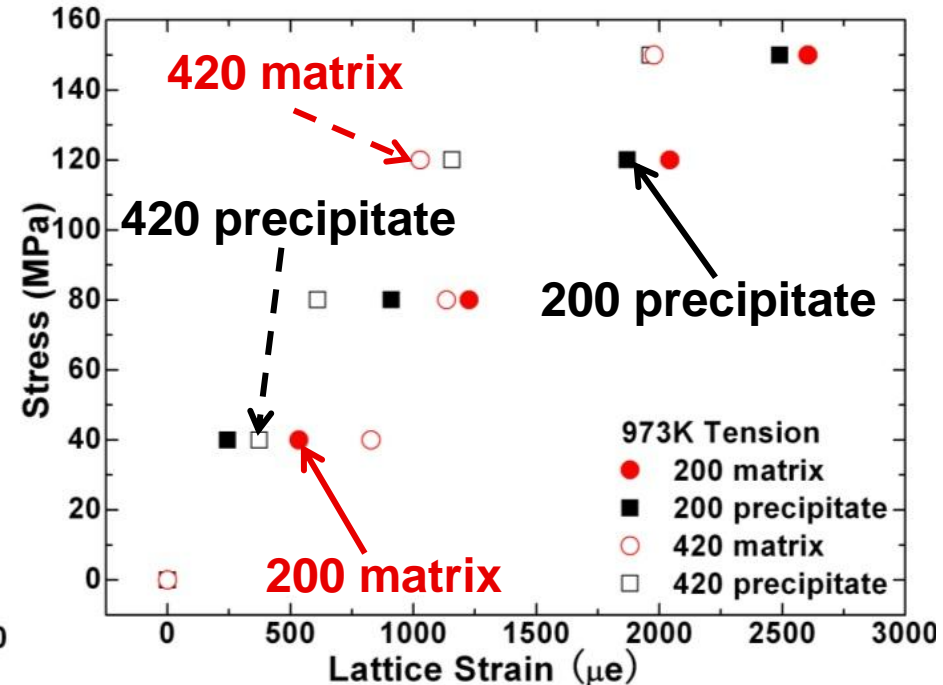
Local phase lattice strain

- Interphase load transfer is superimposed on the intergranular load transfer.

- There is dramatic load transfer from matrix to precipitate phase at 773K, after yielding of most similarly oriented hkl grain families.

6.3 Tension at 873 and 973 K – local phase lattice strain

Local phase lattice strain
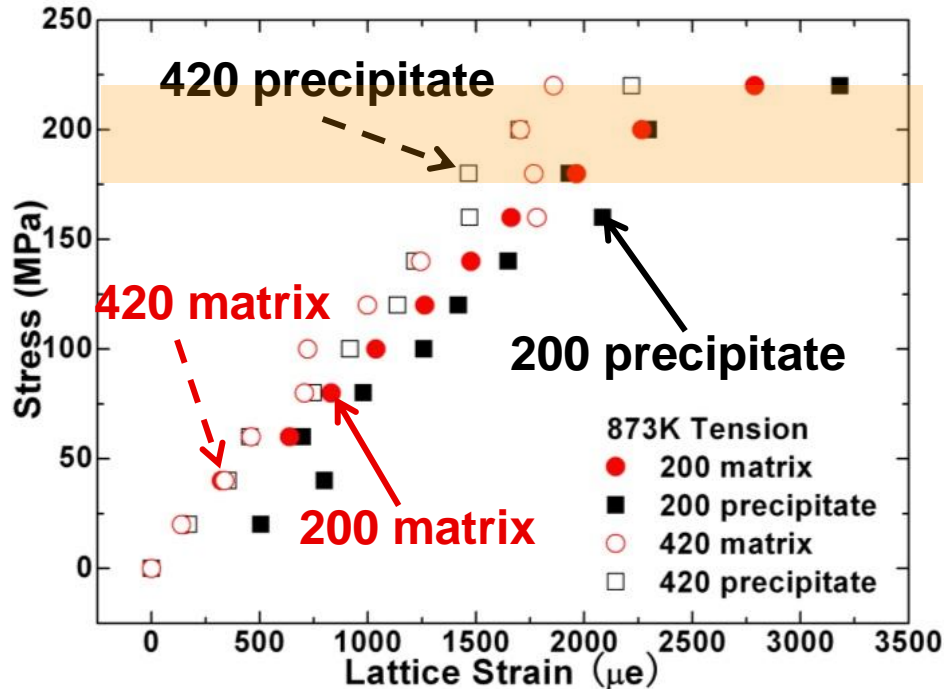
- At 973 K, macroscopic strain increases substantially at high stress levels due to creep. There is no obvious evidence of intergranular and interphase load transfer.

1.1 Calculation of Elastic Constants of Fe, *B2*, and *L2₁* Phases

$$E(V,\{e_i\}) = E(V_0,0) - PV_0\sum_{i=1}^{3} e_i + \frac{V_0}{2}\sum_{i=1}^{6}\sum_{j=1}^{6} C_{ij}e_i e_j + O[e_i^3]$$

• Fe and *B2* Phases (in GPa)

Phase / Elastic Constant	Fe: Cal. (Exp.)	NiAl: Cal. (Exp.)	FeAl: Cal.	CoAl: Cal.
C_{11}	264.37 (243.1*)	207.30 (206.7**)	266.64	292.49
C_{12}	135.10 (138.1*)	135.48 (135.4**)	130.20	123.83
C_{44}	91.21 (121.9*)	116.18 (116.8**)	144.93	135.90

*At 4.2 K: J.A. Rayne and B.S. Chandrasekhar, Phys. Rev., 1960, 120, 1658.
**50 at.% Ni and at 251 K: T. Davenport, L. Zhou and J. Trivisonno, Phys. Rev. B, 1999, 59, 3421.

• Heusler Phases (in GPa)

Phase / Elastic Constant	Co_2TiAl	Fe_2TiAl	Ni_2TiAl
C_{11}	288.89	313.75	211.87
C_{12}	137.79	124.07	143.39
C_{44}	111.88	108.77	87.23

- C_{ij}s are obtained by first-principles method: total energy of the system as a function of deformation ($E(V,\{e_i\})$).
- A comparison of calculated C_{ij} of Fe and B2 phases were given previously in a quarterly progress report*.
- There is NO experimental C_{ij} data of Heusler phases, so calculations from first-principles is the only viable option.
- C_{ij} is needed to understand morphology of coherent precipitates and interfacial energy.

* Report_DOE_DE-FE0005868_07292011.pdf